Calculation of the ^{6}Li ground state within the hyperspherical harmonic basis

A. Gnech [1,2] M. Viviani [2] and L. E. Marcucci[3,2]
[1]*Gran Sasso Science Institute, 67100 L'Aquila, Italy*
[2]*INFN-Pisa, 56127 Pisa, Italy*
[3]*Universitá di Pisa, 56127 Pisa, Italy*

(Received 14 April 2020; revised 22 May 2020; accepted 15 June 2020; published 2 July 2020)

We have studied the solution of the six-nucleon bound state problem using the hyperspherical harmonic (HH) approach. For this study we have considered only two-body nuclear forces. In particular we have used a chiral nuclear potential evolved with the similarity renormalization group unitary transformation. A restricted basis has been selected by performing a careful analysis of the convergence of different HH classes. Finally, the binding energy and other properties of ^{6}Li ground state are calculated and compared with the results obtained by other techniques. Then, we present a calculation of matrix elements relevant for direct dark matter search involving ^{6}Li. The results obtained demonstrate the feasibility of using the HH method to perform calculations beyond $A = 4$.

DOI: 10.1103/PhysRevC.102.014001

I. INTRODUCTION

The *ab initio* description of $A = 6$ nuclear systems, starting from realistic nucleon-nucleon (NN) interaction, requires very large efforts. Indeed, while there are many very well established methods which are able to solve the Schrödinger equation up to $A = 4$ with high precision, very few *ab initio* techniques can be successfully applied to the $A = 6$ problem.

The methods devised to tackle the problem of the solution of the nonrelativistic Schrödinger equation

$$H\Psi = E\Psi, \tag{1}$$

where H is the six-body Hamiltonian, are very different and they usually are not able to deal with the same potentials. In the Green's function Monte Carlo (GFMC) method (see Ref. [1] and references therein), a trial wave function is evolved using a stochastic procedure towards the exact ground state wave function. In this approach only local nuclear interactions can be used. However, up to now it is the only technique that can reach a reasonable convergence beyond $A = 4$ using realistic interactions [2]. The development of unitary transformation methods, such as the similarity renormalization group (SRG) method [3,4], and the increasing power of the computational resources have opened the possibility to successfully apply variational approaches to system with $A > 4$. The unitary transformation methods permit the softening of the short-range repulsion of the nuclear interactions, reducing the dimension of the basis needed to reach convergence. The no-core shell model (NCSM) method [5] performs the calculation by expanding the wave function on the harmonic oscillator (HO) basis and reducing the problem to an eigenvalue problem. The use of evolved nuclear potentials does not allow a direct comparison of the NCSM and GFMC results, because of the emergence in the SRG procedure of many-body forces that are not usually fully included. The effective interaction hyperspherical harmonics (EIHH) method [6] adopts another type of unitary transformation in which the full Hamiltonian of Eq. (1) is replaced with the transformed one, which is easier to solve, and the calculated eigenvalues quickly converge to the exact ones. The results for $A = 6$ systems have been obtained with central potentials [6], and more recently with nonlocal NN interactions [7]. Other explorative studies in the $A = 6$ sector using the hyperspherical harmonics (HH) approach were performed in Refs. [8,9]. In Ref. [8], the HH are symmetrized by using the Casimir operators, and the calculations are performed using the JISP16 [10] nonlocal interaction. In Ref. [9], the nonsymmetrized hyperspherical harmonics (NSHH) are used with the Volkov [11] potential. Other results for ^{6}Li were obtained by using the stochastic variational method (SVM) [12], where only central potentials without the full complication of the modern chiral interactions were used. Also the solution of $A = 5, 6$ with the Faddeev-Yakoubovsky (FY) equation is vigorously explored [13,14].

In the present work we address the problem of calculating the ^{6}Li properties, using a nuclear Hamiltonian containing only two-body chiral interactions evolved with the SRG unitary transformation, within the HH approach. Our goal is to reach reliable convergences with these potentials and perform solid extrapolations of the nuclear observables. The motivation is twofold. First, we would like to show that the HH approach, as developed by the Pisa group [15,16], can be successfully applied for nuclei with $A > 4$. Therefore, this work can be considered as the first step which will permit studying a variety of phenomena in $A = 6$ sector with the HH method. Second, we would like to perform a comparison with the results obtained by the NCSM method. In this

sense, this work would represent an important independent benchmark which validates in the $A = 6$ sector both the approaches.

The main problem of using the HH expansion is related to the slow convergence of the basis. In the present case, this problem is enhanced by the fact that the nucleus of ^{6}Li is strongly clustered in an α particle and a deuteron (d). Indeed, the HH basis, being very compact, has some difficulties in describing clustered structures. This requires one to include a large number of antisymmetric spin-isospin HH states to reach a good convergence even with very soft potential, as in the case of the SRG evolved ones. Indeed, the expansion in HH states, which is controlled by the grand-angular quantum number K (see below), involves more than 10^4 states already for $K = 6$ and they increase exponentially as K grows. It is clear that a brute force approach is not possible even with sophisticated computational facilities. The idea is to select a suitable subsets of states as proposed in Refs. [17–21]. Here, we use an approach very similar to the one used in Ref. [21] for the α particle, where the HH states were selected in terms of the sum of the particles' angular momentum and the number of correlated particles. This classification permits one to define subsets of states (hereafter named "classes") having similar properties, so as to optimize the expansion basis. In the following, we will carefully analyze the convergence of each class, so as to have an accurate calculation of the ^{6}Li ground state properties.

The successful application of the HH method is permitted by the use of the coefficients for the transformation of the HH functions from a generic permutation of the six particles to a reference one. To obtain these coefficients, we used the same approach of Refs. [22,23] extending it for six particles. The use of the coefficients permits us to identify and eliminate the linear dependent states from the basis. The elimination of these "spurious states" is very useful, since the number of linear independent states is noticeably smaller than the full degeneracy of the basis. Moreover, through the coefficients, the potential matrix elements can be computed easily and with high accuracy, performing only one (two) integration(s) for local (nonlocal) two-body potentials.

The study presented in this article is the direct extension of the calculation of Ref. [21] performed on $A = 4$ nucleon systems, where the use of the same approach for systems with $A > 4$ was already predicted. The natural continuation will be the inclusion of three-body forces and the attempt of using also "bare" chiral interactions. These two lines of research are currently under way. Moreover, we expect that it will be possible to extend the same approach to nuclei up to $A = 8$.

This article is organized as follows. In Sec. II we briefly introduce the HH formalism for $A = 6$. In Sec. III we present the selection of the HH basis. The convergence of the binding energy and the study of ^{6}Li ground state properties are presented in Sec. IV. In Sec. V the matrix elements relevant for direct dark matter search with ^{6}Li are studied. The last section is dedicated to the conclusions and the perspectives of the present study. Some of the technical details of the calculation are reported in two appendices.

II. THE HH EXPANSION

The reference set of Jacobi vectors for six equal-mass particles, that we use in this work, is

$$\begin{aligned}
\boldsymbol{\xi}_{1p} &= \sqrt{\frac{5}{3}}\left(\boldsymbol{r}_n - \frac{\boldsymbol{r}_m + \boldsymbol{r}_l + \boldsymbol{r}_k + \boldsymbol{r}_j + \boldsymbol{r}_i}{5}\right),\\
\boldsymbol{\xi}_{2p} &= \sqrt{\frac{8}{5}}\left(\boldsymbol{r}_m - \frac{\boldsymbol{r}_l + \boldsymbol{r}_k + \boldsymbol{r}_j + \boldsymbol{r}_i}{4}\right),\\
\boldsymbol{\xi}_{3p} &= \sqrt{\frac{3}{2}}\left(\boldsymbol{r}_l - \frac{\boldsymbol{r}_k + \boldsymbol{r}_j + \boldsymbol{r}_i}{3}\right),\\
\boldsymbol{\xi}_{4p} &= \sqrt{\frac{4}{3}}\left(\boldsymbol{r}_k - \frac{\boldsymbol{r}_j + \boldsymbol{r}_i}{2}\right),\\
\boldsymbol{\xi}_{5p} &= \boldsymbol{r}_j - \boldsymbol{r}_i,
\end{aligned} \tag{2}$$

where (i, j, k, l, m, n) indicates a generic permutation p of the particles. By definition $p = 1$ is chosen to correspond to (1,2,3,4,5,6). In the following, the "standard" set of Jacobi vectors will be defined to correspond to this particular definition.

For a given choice of the Jacobi vectors, the hyperspherical coordinates are given by the hyperradius ρ, which is independent of the permutation p of the particles and is defined as

$$\rho = \sqrt{\sum_{i=1,N} \xi_{ip}^2}, \tag{3}$$

and by a set of variables, which in the Zernike and Brinkman representation [20,24] are the polar angles $\hat{\xi}_{ip} = (\theta_{ip}, \phi_{ip})$ of each Jacobi vector and the four additional "hyperspherical" angles φ_{jp}, with $j = 2, \ldots, 5$, defined as

$$\cos\varphi_{jp} = \frac{\xi_{jp}}{\sqrt{\xi_{1p}^2 + \cdots + \xi_{jp}^2}}, \tag{4}$$

where ξ_{jp} is the modulus of the Jacobi vector $\boldsymbol{\xi}_{jp}$. The set of variables $\hat{\xi}_{1p}, \ldots, \hat{\xi}_{5p}, \varphi_{2p}, \ldots, \varphi_{5p}$ is denoted hereafter as Ω_p. The expression of the generic HH function is

$$\begin{aligned}
\mathcal{Y}_\mu^{KLM}(\Omega_p) = \Big[\Big(\Big\{\Big[Y_{\ell_1}(\hat{\xi}_{1p})Y_{\ell_2}(\hat{\xi}_{2p})\Big]_{L_2} Y_{\ell_3}(\hat{\xi}_{3p})\Big\}_{L_3}\\
\times Y_{\ell_4}(\hat{\xi}_{4p})\Big)_{L_4} Y_{\ell_5}(\hat{\xi}_{5p})\Big]_{LM}\\
\times \mathcal{P}^{\ell_1,\ell_2,\ell_3,\ell_4,\ell_5}_{n_2,n_3,n_4,n_5}(\varphi_{2p}, \varphi_{3p}, \varphi_{4p}, \varphi_{5p}),
\end{aligned} \tag{5}$$

where

$$\begin{aligned}
&\mathcal{P}^{\ell_1,\ell_2,\ell_3.\ell_4,\ell_5}_{n_2,n_3,n_4,n_5}(\varphi_{2p}, \varphi_{3p}, \varphi_{4p}, \varphi_{5p})\\
&= \mathcal{N}^{\ell_2,\nu_2}_{n_2}(\cos\varphi_{2p})^{\ell_2}(\sin\varphi_{2p})^{\ell_1} P^{\ell_1+1/2,\ell_2+1/2}_{n_2}(\cos 2\varphi_{2p})\\
&\times \mathcal{N}^{\ell_3,\nu_3}_{n_3}(\cos\varphi_{3p})^{\ell_3}(\sin\varphi_{3p})^{K_2} P^{\nu_2,\ell_3+1/2}_{n_3}(\cos 2\varphi_{3p})\\
&\times \mathcal{N}^{\ell_4,\nu_4}_{n_4}(\cos\varphi_{4p})^{\ell_4}(\sin\varphi_{4p})^{K_3} P^{\nu_3,\ell_4+1/2}_{n_4}(\cos 2\varphi_{4p})\\
&\times \mathcal{N}^{\ell_5,\nu_5}_{n_5}(\cos\varphi_{5p})^{\ell_5}(\sin\varphi_{5p})^{K_4} P^{\nu_4,\ell_5+1/2}_{n_5}(\cos 2\varphi_{5p}),
\end{aligned} \tag{6}$$

and $P_n^{a,b}$ are Jacobi polynomials. The coefficients $\mathcal{N}_{n_j}^{\ell_j,\nu_j}$ are normalization factors given explicitly by

$$\mathcal{N}_{n_j}^{\ell_j,\nu_j} = \left[\frac{2\nu_j\Gamma(\nu_j - n_j)n_j!}{\Gamma\left(\nu_j - n_j - \ell_j - \frac{1}{2}\right)\Gamma\left(n_j + \ell_j + \frac{3}{2}\right)}\right]^{1/2}, \quad (7)$$

where we have defined

$$K_j = \ell_j + 2n_j + K_{j-1}, \qquad \nu_j = K_j + \frac{3}{2}j - 1, \quad (8)$$

with $K_1 = \ell_1$ and $K_5 = K$. The integer index μ labels the choice of all the hyperangular quantum numbers, namely

$$\mu \equiv \{\ell_1, \ell_2, \ell_3, \ell_4, \ell_5, L_2, L_3, L_4, n_2, n_3, n_4, n_5\}. \quad (9)$$

The kinetic energy operator for the six particles, without the center-of-mass (c.m.) motion, can be rewritten in term of the variables $\{\rho, \Omega_p\}$ as

$$\sum_{j=1,5}\nabla_j^2 = \left[\frac{\partial^2}{\partial\rho^2} + \frac{14}{\rho}\frac{\partial}{\partial\rho} + \frac{\Lambda^2(\Omega_p)}{\rho^2}\right], \quad (10)$$

where $\Lambda^2(\Omega_p)$ is called the grand-angular momentum operator and depends only on the hyperangular coordinates. The HH functions are the eigenfunctions of this operator, namely

$$[\Lambda^2(\Omega_p) + K(K+13)]\mathcal{Y}_\mu^{KLM}(\Omega_p) = 0, \quad (11)$$

where with K we indicate the eigenvalue of this operator, which is usually called grand-angular quantum number.

Our wave function is constructed to have a well defined total angular momentum J, J_z, parity π, and isospin T (in the following, we disregard small admixtures between isospin states). Therefore, we define a complete basis of antisymmetrical hyperangular-spin-isospin states as follows:

$$\Psi_\alpha^{KLSTJ\pi} = \sum_{p=1}^{360}\Phi_\alpha^{KLSTJ\pi}(i, j, k, l, m, n), \quad (12)$$

where the sum is over the 360 even permutations p of the particles and

$$\Phi_\alpha^{KLSTJ\pi}(i, j, k, l, m, n) = \left\{\mathcal{Y}_\mu^{KLM}(\Omega_p)[[[s_i s_j]_{S_2} s_k]_{S_3} \times [[s_l s_m]_{S_4} s_n]_{S_5}]_S\right\}_{JJ_z}[[[t_i t_j]_{T_2} t_k]_{T_3} \times [[t_l t_m]_{T_4} t_n]_{T_5}]_{TT_z}. \quad (13)$$

The function $\mathcal{Y}_\mu^{KLM}(\Omega_p)$ is the HH function defined in Eq. (5) and s_i (t_i) denotes the spin (isospin) function of nucleon i. Note that the coupling scheme of the spin (isospin) states does not follow the one of the hyperangular part. This particular choice simplifies the calculation of the potential matrix elements. There are other possible choices for the coupling of the spin (isospin) states that can be easily connected to our choice through combinations of $6j$- and $9j$-Wigner coefficients. The total orbital angular momentum L of the HH function is coupled to the total spin S to give the total angular momentum J, J_z, while the total isospin is given by T, T_z. The index α labels the possible choice of hyperangular, spin, and isospin quantum numbers, namely

$$\alpha \equiv \{\ell_1, \ell_2, \ell_3, \ell_4, \ell_5, L_2, L_3, L_4, n_2, n_3, n_4, n_5, \times S_2, S_3, S_4, S_5, T_2, T_3, T_4, T_5\}, \quad (14)$$

compatible with the given values of K, L, S, T, J, and π. The parity of the state is defined by $\pi = (-1)^{\ell_1+\ell_2+\ell_3+\ell_4+\ell_5}$ and we will include in our basis only the states such that π corresponds to the parity of the nuclear state under study.

The total wave function must be completely antisymmetric under exchange of any pair of particles. Therefore, we need to impose antisymmetry on each state $\Psi_\alpha^{KLSTJ\pi}$. For example, after the permutation of any pair, the state given in Eq. (12) can be rearranged so that

$$\Psi_\alpha^{KLSTJ\pi} \to \sum_{p=1}^{360}\Phi_\alpha^{KLSTJ\pi}(j, i, k, l, m, n). \quad (15)$$

Therefore, to have antisymmetry it is sufficient to impose

$$\Phi_\alpha^{KLSTJ\pi}(j, i, k, l, m, n) = -\Phi_\alpha^{KLSTJ\pi}(i, j, k, l, m, n). \quad (16)$$

Under the exchange of $i \leftrightarrow j$ the Jacobi vector $\boldsymbol{\xi}_{5p}$ [Eq. (2)] changes its sign, whereas all the others remain the same. Therefore, the HH function $\mathcal{Y}_\mu^{KLM}(\Omega_p)$ in Eq. (5) transforms into itself times a factor $(-1)^{\ell_5}$. Under the $i \leftrightarrow j$ exchange, the spin-isospin part [see Eq. (13)] transforms into itself times a factor $(-1)^{S_2+T_2}$. In conclusion the condition in Eq. (16) is fulfilled when

$$\ell_5 + S_2 + T_2 = \text{odd}; \quad (17)$$

that is the condition we impose on the quantum numbers to obtain only antisymmetric states.

The number $M_{KLSTJ\pi}$ of antisymmetric functions $\Psi_\alpha^{KLSTJ\pi}$ with fixed K, L, S, T, J, and π in general is very large, due to the high number of possible combinations of quantum numbers α that fulfill the requirements of antisymmetry and parity. However, states constructed in such a way are linearly dependent among each other. In the expansion of the wave function, it is necessary to include the linearly independent states only. The fundamental ingredient to identify the independent states is the knowledge of the norm matrix elements

$$N_{\alpha,\alpha'}^{KLSTJ\pi} = \left\langle\Psi_\alpha^{KLSTJ\pi}\middle|\Psi_{\alpha'}^{KLSTJ\pi}\right\rangle_\Omega, \quad (18)$$

where $\langle\rangle_\Omega$ denotes the spin and isospin trace and the integration over the hyperspherical variables. The calculation of the above matrix elements, and also those of the Hamiltonian (see below), is considerably simplified by using the transformation

$$\Phi_\alpha^{KLSTJ\pi}(i, j, k, l, m, n) = \sum_{\alpha'} a_{\alpha,\alpha'}^{KLSTJ\pi}(p)\Phi_{\alpha'}^{KLSTJ\pi}(1, 2, 3, 4, 5, 6). \quad (19)$$

The coefficients $a_{\alpha,\alpha'}^{KLSTJ\pi}(p)$ have been obtained using the techniques described in Refs. [22,23], generalized to the $A = 6$ case. Hence, the states $\Psi_\alpha^{KLSTJ\pi}$ of Eq. (12) can be written as

$$\Psi_\alpha^{KLSTJ\pi} = \sum_{\alpha'} A_{\alpha,\alpha'}^{KLSTJ\pi}\Phi_{\alpha'}^{KLSTJ\pi}(1, 2, 3, 4, 5, 6), \quad (20)$$

where

$$A_{\alpha,\alpha'}^{KLSTJ\pi} = \sum_{p=1}^{360} a_{\alpha,\alpha'}^{KLSTJ\pi}(p). \quad (21)$$

TABLE I. Number of six-nucleon antisymmetrical hyperspherical-spin-isospin states for the case $J = 1$, $\pi = +$, $T = 0$, and $L = 0$ and 2 for various cases of the grand-angular quantum number K and the total spin S. $M_{KLSTJ\pi}$ is the total number of antisymmetric states while $M'_{KLSTJ\pi}$ is the number of independent antisymmetric states. With the * we indicate that the reported value of $M'_{KLSTJ\pi}$ is underestimated since probably there are other independent states that must be included to determine the complete basis.

	$L=0,\ S=1$		$L=2,\ S=1$		$L=2,\ S=2$		$L=2,\ S=3$	
K	M_{K0101+}	M'_{K0101+}	M_{K2101+}	M'_{K2101+}	M_{K2201+}	M'_{K2201+}	M_{K2301+}	M'_{K2301+}
0	21	0						
2	306	1	327	1	177	0	34	0
4	2 325	7	4 662	12	2 562	4	504	1
6	12 480	34	34 065	90	18 815	42	3 730	9
8	52 893	144	172 500	442	95 500	227	19 000	46
10	187 842	509	684 885	1535*	379 635	804*	75 670	145
12	580 767		2 280 030		1 264 730		252 360	
14	1 605 588							

The coefficients $A^{KLSTJ\pi}_{\alpha,\alpha'}$ are called transformation coefficients (TCs) and contain all the properties of our basis. Therefore, the knowledge of all of them coincides with the knowledge of the entire basis. By using them, the matrix element of the norm can be easily obtained by taking advantage of the orthogonality of the HH basis, namely

$$N^{KLSTJ\pi}_{\alpha,\alpha'} = \sum_{\alpha''} \left(A^{KLSTJ\pi}_{\alpha,\alpha''}\right)^* A^{KLSTJ\pi}_{\alpha',\alpha''}. \tag{22}$$

Clearly,

$$\left\langle \Psi^{KLSTJ\pi}_{\alpha} \middle| \Psi^{K'L'S'T'J'\pi'}_{\alpha'} \right\rangle_{\Omega} = 0, \tag{23}$$

if $\{KLSTJ\pi\} \neq \{K'L'S'T'J'\pi'\}$. Once the matrix elements $N^{KLSTJ\pi}_{\alpha,\alpha'}$ are evaluated, the Gram-Schmidt procedure is used to find and eliminate the linearly dependent states among the various $\Psi^{KLSTJ\pi}_{\alpha}$ functions.

We have found that the number of independent antisymmetric states $M'_{KLSTJ\pi}$ is noticeably smaller than the corresponding $M_{KLSTJ\pi}$. For example, in Table I we report the values of $M_{KLSTJ\pi}$ and $M'_{KLSTJ\pi}$ for the case $J = 1$, $T = 0$, $L = 0$ and 2, and $\pi = +$, which corresponds to the main components of the ^{6}Li ground state. Observing the table it is possible to note that the values of M_{KLS01+} start to be very large already for $K = 6$ while those M'_{KLS01+} are much smaller. For the case $K = 0$ and $LSTJ\pi = 0101+$, there are no independent states due to the Pauli principle.

The final form of the six-nucleon bound state wave function can be written as

$$\Psi^{J\pi}_{6} = \sum_{l} \sum_{KLST,\alpha} c^{KLST}_{l,\alpha} f_l(\rho) \Psi^{KLSTJ\pi}_{\alpha}, \tag{24}$$

where the sum is restricted only to the linear independent antisymmetric states α, and $c^{KLST}_{l,\alpha}$ are variational coefficients to be determined. The hyperradial functions $f_l(\rho)$ are chosen to be

$$f_l(\rho) = \gamma^{15/2} \sqrt{\frac{l!}{(l+14)!}}\ L^{(14)}_l(\gamma\rho)\, e^{-\frac{\gamma}{2}\rho}, \tag{25}$$

where $L^{(14)}_l(\gamma\rho)$ are Laguerre polynomials [25] and γ is a nonlinear variational parameter to be optimized in order to have a fast convergence on l. A typical range for γ is 3.5–5.5 fm^{-1}. The expansion coefficients $c^{KLST}_{l,\alpha}$ are determined using the Rayleigh-Ritz variational principle, which leads to

$$\sum_{\beta'} \langle \Psi_\beta | H | \Psi_{\beta'} \rangle c_{\beta'} = E \sum_{\beta'} c_{\beta'} \langle \Psi_\beta | \Psi_{\beta'} \rangle, \tag{26}$$

where $\beta = \{K, L, S, T, l, \alpha\}$ and $\Psi_\beta = f_l(\rho)\Psi^{KLSTJ\pi}_{\alpha}$. The eigenvalue problem in Eq. (26) is then solved by using the procedure of Ref. [26]. The computation of the Hamiltonian matrix elements is straightforward for the norm $\langle \Psi_\beta | \Psi_{\beta'} \rangle$ by using Eq. (22), and also for the kinetic energy, since we are using the eigenbasis of the kinetic energy operator. The calculation of the potential matrix elements is more involved and is discussed in Appendix A.

III. CHOICE OF THE BASIS

The main difficulty of the HH method is the selection of a subset of basis states allowing for the best description of the nuclear states we are considering. Indeed, although the number of independent states is much smaller than the degeneracy of the basis, the brute force approach of the method—that is, the inclusion of all the HH states having $K \leqslant K_M$ and then increasing K_M until convergence—would be doomed to fail. Moreover, it is very difficult to find all the linearly independent states already for values of $K = 10$, because of the loss of precision in the orthogonalization procedure. For this reason, a good selection of a restricted and effective subset of basis states is fundamental. Up to now we are limited to values $K_M \leqslant 14$, which permits reaching a reasonable convergence only for "soft" core potentials, as in the case of the SRG evolved ones.

It is convenient to separate the HH functions into classes, taking into account their properties and the fact that the convergence rate of each class is rather different. The first selection can be done considering the quantity $\ell_{\rm sum} = \ell_1 + \ell_2 + \ell_3 + \ell_4 + \ell_5$. Indeed, the HH states with large $\ell_{\rm sum}$ are less correlated by the NN potential because of the centrifugal barrier. The SRG potentials have quite weak correlations and so, in our calculation, we can consider states with only $\ell_{\rm sum} \leqslant 4$. A second criterion which can be used is to consider the number of particles correlated by the HH functions. The

TABLE II. Definition of the classes of hyperangular-spin-isospin states $\Psi_\alpha^{KLSTJ\pi}$ [see Eq. (12)] used to study the ^{6}Li bound state. The classes are defined by selecting particular values of the total orbital angular momentum L, of the total spin S, and of the value of $\ell_{\rm sum} = \ell_1 + \cdots + \ell_5$, given in the second and third columns, respectively (the values for L and S are shown using the spectroscopic notation). In this work we have retained states with $T = 0$ only. As an example, class C1 includes states $\Psi_\alpha^{KLSTJ\pi}$ with $L = 0$, $S = 1$, $T = 0$, $\ell_{1-5} = 0$, and all possible combinations of the remaining quantum numbers compatible with $K \leqslant K_{1M}$ [see Eq. (14)]. In the last column, the maximum value of K used in the expansion for each class is also reported.

Class	Partial waves	$\ell_{\rm sum}$	K_{iM}
C1	$^3S_1$	$\ell_{\rm sum} = 0$	14
C2	$^3D_1, ^5D_1, ^7D_1$	$\ell_5 = 2, \sum_{i=1,4} \ell_i = 0$	12
C3	$^3S_1$	$\ell_{\rm sum} = 2$	10
C4	$^3D_1, ^5D_1, ^7D_1$	$\ell_{\rm sum} = 2$ not included in C2	10
C5	$^1P_1, ^3P_1, ^5P_1$	$\ell_{\rm sum} = 2$	8
C6	$^5F_1, ^7F_1, ^7G_1$	$\ell_{\rm sum} = 4$	8

nuclear potential favors the two-body correlations; therefore the HH states which depend only on the coordinates of a couple of particles give the main contributions. A typical example is HH states with only n_5 and ℓ_5 not zero. However, for simplicity, in the following we will use the criterion on $\ell_{\rm sum}$ for the class definition. Moreover, the ^{6}Li ground state can be divided into LST components, which we used as well to define the classes. Since the ^{6}Li ground state is an almost pure $T = 0$ state, we do not consider other isospin states. The properties of the HH states which define the classes are summarized in Table II. For each class i we report also the maximum value K_{iM} we need to reach to obtain convergence in the binding energy (last column of Table II). As can be noticed by inspecting the table, the maximum values for K_{iM} must be reached for classes C1 and C2, since they represent the main component of the ^{6}Li ground state. Classes C3 and C4 contains only many-body correlations. Therefore, their impact on the binding energy is less significant and we obtain a reasonable convergence for $K_{3M} = K_{4M} = 10$. Classes C5 and C6 are the less important since their contribution to the binding energy is quite small. For them we stop up to $K_{5M} = K_{6M} = 8$.

Moreover, for the classes C3 and C4, starting from $K_{iM} \geqslant 10$, we need to perform a precision truncation. Namely, due to the loss of numerical precision in the orthogonalization procedure, states with small orthogonal component generate "spurious" bound states when we diagonalize the Hamiltonian. Therefore, we perform a truncation of the basis that avoids the generation of these spurious bound states. As it will be clear below, the contribution of these classes is very small and so the truncation is practically irrelevant on the final extrapolation of the binding energy. We want to underline that with this selection of the classes, up to $K = 8$ the HH basis is complete. The convergence is studied as follows. First, only the states of class C1 with $K \leqslant K_1$ are included in the expansion, and the convergence of the binding energy is studied as the value of K_1 is increased up to K_{1M}. Once a satisfactory convergence for the first class is reached, the states of the second class with $K \leqslant K_2$ are added to the expansion, keeping all the states of the class C1 with $K \leqslant K_{1M}$. The procedure is then repeated for each new class. Our complete calculation includes about 7000 HH states.

IV. RESULTS FOR THE ^{6}Li GROUND STATE

In this section we report the results obtained for the ground state of ^{6}Li. In this work we have used $\hbar^2/m = 41.47$ MeV fm^2 for all the potentials. Moreover, we use $\gamma = 4$ fm^{-1} in the hyperradial functions [see Eq. (25)]. This value has been found optimal in order to reach convergence to the third decimal digit with a number of Laguerre polynomials $l_{\rm max} = 16$. For all the considered models, when the angular momentum of the pair j is large, the NN interactions effect is very small. Therefore, all the interactions for $j > 6$ are discarded, since their effects are negligible as already shown in Ref. [21] for the α particle.

This section is divided into four parts. The validation of our approach is shown in Sec. IV A, comparing our results with the ones obtained in Ref. [9]. In Sec. IV B, we discuss the convergence of the HH expansion in terms of the various classes for the SRG evolved potentials. The electromagnetic static properties of the ^{6}Li ground state are considered in Sec. IV C. Finally, the calculation of the ^{6}Li asymptotic normalization coefficients is presented in Sec. IV D.

A. Validation of the results

In order to validate our calculation we have performed a benchmark with the results presented in Ref. [9], obtained with the nonsymmetrized HH (NSHH) approach. We perform the benchmark by using the Volkov potential [11]

$$V(r) = V_R e^{-r^2/R_1^2} + V_A e^{-r^2/R_2^2}, \tag{27}$$

where $V_R = 144.86$ MeV, $R_1 = 0.82$ fm, $V_A = -83.34$ MeV, and $R_2 = 1.6$ fm. Since the Volkov potential is a central potential, it does not couple the different partial wave components of the wave function. Therefore, we consider only the $L = 0$, $S = 1$, and $T = 0$ component which corresponds to classes C1 and C3. For this study we consider states of class C3 up to $K_{3M} = 12$. In such a way, we are using exactly the same expansion of Ref. [9] for $K \leqslant 12$.

TABLE III. Binding energy of the bound state of $A = 6$ as a function of the grand-angular momentum K obtained with the Volkov potential. The first two columns are the results obtained in this work considering class C1 and class C1+C3 respectively. In the third column we report the results of Ref. [9].

K_{iM}	C1	C1+C3	Ref. [9]
2	−61.142	−61.142	−61.142
4	−62.015	−62.015	−62.015
6	−63.377	−63.377	−63.377
8	−64.415	−64.437	−64.437
10	−65.310	−65.354	−65.354
12	−65.823	−65.884	−65.886

TABLE IV. Convergence of ^{6}Li binding energies (MeV) corresponding to the inclusion in the wave function of the different classes C1–C6, into which the HH basis has been divided. The SRG-evolution parameters correspond to $\Lambda = 1.2$, 1.5, and 1.8 fm^{-1}.

						N3LO500-SRGΛ		
K_1	K_2	K_3	K_4	K_5	K_6	1.2 fm^{-1}	1.5 fm^{-1}	1.8 fm^{-1}
2						24.779	22.315	17.946
4						28.606	26.779	22.656
6						29.714	28.395	24.646
8						30.030	28.937	25.425
10						30.150	29.159	25.781
12						30.195	29.254	25.948
14						30.213	29.295	26.031
14	2					30.263	29.362	26.108
14	4					30.900	30.481	27.619
14	6					31.318	31.626	29.819
14	8					31.413	32.006	30.827
14	10					31.437	32.122	31.195
14	12					31.444	32.167	31.352
14	12	6				31.445	32.168	31.354
14	12	8				31.477	32.210	31.396
14	12	10				31.493	32.233	31.422
14	12	10	4			31.501	32.245	31.437
14	12	10	6			31.550	32.329	31.548
14	12	10	8			31.577	32.389	31.642
14	12	10	10			31.586	32.412	31.689
14	12	10	10	2		31.658	32.533	31.836
14	12	10	10	4		31.710	32.631	31.970
14	12	10	10	6		31.728	32.677	32.047
14	12	10	10	8		31.735	32.699	32.093
14	12	10	10	8	4	31.736	32.703	32.101
14	12	10	10	8	6	31.746	32.733	32.161
14	12	10	10	8	8	31.750	32.751	32.209

In Table III we report the binding energy of the bound state of $A = 6$ as function of the grand-angular momentum K for classes C1 and C1+C3. As can be seen from the table, if we use only the HH states which belong to class C1 we are not able to reproduce the results of Ref. [9], even if only few tens of keV are missing. Once we add the HH states belonging to class C3 up to $K = 10$ we recover the values of Ref. [9], as we expect, since we are using exactly the same basis. As can be seen, the precision truncation performed on the class C3 for $K = 10$ is irrelevant. This is not the case of $K = 12$, where a 2 keV difference remains, due to the fact we are not including states with $\ell_{\rm sum} = 4$ because of the truncation precision. We want to remark that, despite this truncation, only 2 keV are missing for $K = 12$, well below the precision of the convergence on K.

B. Convergence of the HH expansion

We study the convergence as explained in Sec. III, and the results presented are arranged accordingly. For example, in Table IV, the binding energy reported in a row with a given set of values $K_1, \ldots, K_6$ has been obtained by including in the expansion all the HH functions of class Ci with $K \leqslant K_i$, $i = 1, \ldots, 6$. In the following, we considered the N3LO500 chiral potential of Entem and Machleidt [27], SRG-evolved with $\Lambda = 1.2$, 1.5, 1.8 fm^{-1} [3]. The Coulomb interaction is included as "bare" (i.e., not SRG evolved). We want to remark that these results are obtained considering only two-body forces.

We can now analyze the results in Table IV. We observe that classes C1 and C2 are the most important and have the slowest convergence. Indeed the largest values of K must be reached. It is evident that, for increasing value of the SRG parameter Λ, the convergence becomes slower. This is due to the "hardness" of the potential that is enhanced when Λ is large. Moreover, class C2 becomes less and less significant when Λ becomes smaller. This effect is generated by the SRG evolution, which reduces the correlations between the S and D waves, when Λ decreases. Even if they are the slowest converging classes, they give 98% of the binding energy. The contribution of classes C3 and C4 is very small for all the values of the flow parameters Λ, and also the convergence is much faster. It is very interesting to observe that for both classes the contribution to the binding energy depends much less on the value of Λ compared to that of classes C1 and C2. This gives an indication that the many-body correlations are not very important, independently of the SRG evolution parameter. We find also that class C5, which corresponds to P waves, and class C6, which corresponds to F and G waves, give very small contributions to the ground state of ^{6}Li. Indeed, in order to obtain the same convergence of the other classes, we can stop at $K_{5M} = K_{6M} = 8$.

Let us comment about the convergence rate as function of the maximum grand-angular quantum number K_{iM} of the various classes of HH states included in our expansion. As shown in various studies [19,20,28,29], the convergence of the HH functions towards the exact binding energy depends primarily on the form of the potential. For the chiral potentials, it was observed empirically that the convergence rate has an exponential behavior as K_i increases. We expect that the same rate of the convergence is obtained also for the SRG evolved potentials as already observed for example in Ref. [30], even if it was obtained within the harmonic oscillator basis.

In order to study the convergence behavior, we indicate with $B(K_1, K_2, K_3, K_4, K_5, K_6)$ the binding energy obtained by including in the expansion all the HH states of class C1 with $K \leqslant K_1$, all the HH states of class C2 having $K \leqslant K_2$, and so on. Let us define

$$\Delta_1(K) = B(K, K_{2M}, 0, K_{4M}, K_{5M}, K_{6M}) - B(K-2, K_{2M}, 0, K_{4M}, K_{5M}, K_{6M}), \quad (28)$$

$$\Delta_2(K) = B(K_{1M}, K, K_{3M}, 0, K_{5M}, K_{6M}) - B(K_{1M}, K-2, K_{3M}, 0, K_{5M}, K_{6M}), \quad (29)$$

$$\Delta_3(K) = B(K_{1M}, K_{2M}, K, K_{4M}, K_{5M}, K_{6M}) - B(K_{1M}, K_{2M}, K-2, K_{4M}, K_{5M}, K_{6M}), \quad (30)$$

$$\Delta_4(K) = B(K_{1M}, K_{2M}, K_{3M}, K, K_{5M}, K_{6M}) - B(K_{1M}, K_{2M}, K_{3M}, K-2, K_{5M}, K_{6M}), \quad (31)$$

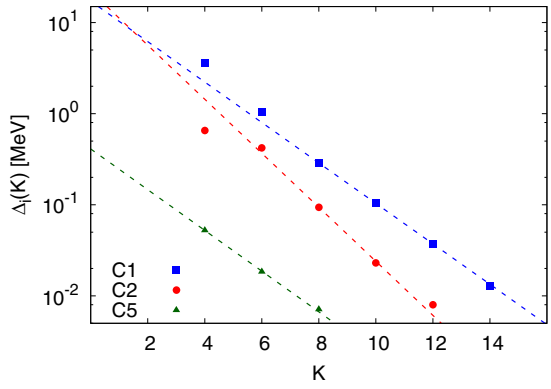

(a) SRG1.2

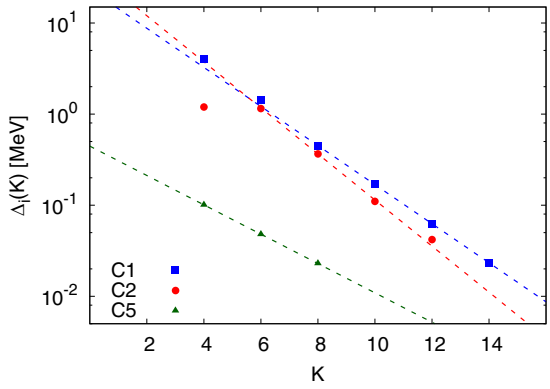

(b) SRG1.5

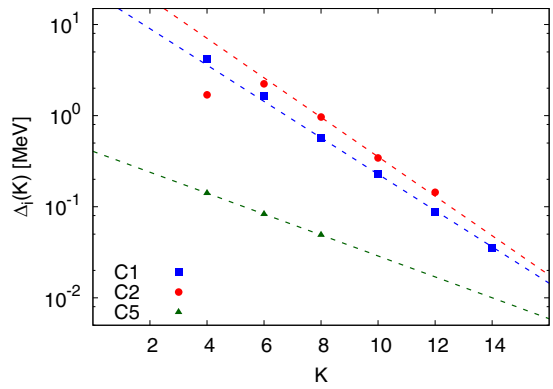

(c) SRG1.8

FIG. 1. Values of Δ_i [see Eqs. (28)–(33)] for the classes C1 (squares), C2 (circles), and C5 (triangles) as function of the grand-angular value K for the three SRG evolved potentials $\Lambda = 1.2$ fm^{-1} (a), $\Lambda = 1.5$ fm^{-1} (b), and $\Lambda = 1.8$ fm^{-1} (c). The dashed lines are the fits obtained using Eq. (35).

$$\Delta_5(K) = B(K_{1M}, K_{2M}, K_{3M}, K_{4M}, K, K_{6M}) - B(K_{1M}, K_{2M}, K_{3M}, K_{4M}, K-2, K_{6M}), \quad (32)$$

$$\Delta_6(K) = B(K_{1M}, K_{2M}, K_{3M}, K_{4M}, K_{5M}, K) - B(K_{1M}, K_{2M}, K_{3M}, K_{4M}, K_{5M}, K-2), \quad (33)$$

where with K_{iM} we indicate that, for the class Ci, we are including all the HH states up to the maximum K considered in this work. With these definitions, we can compute the "missing" binding energy for each class due to the truncation of the expansion up to a given K_i, by taking care of the modifications of convergence of a class Ci due to the inclusion of the other classes. Note that for Δ_1 (Δ_2) we put $K_3 = 0$ ($K_4 = 0$). This is because the HH states included in class C3 (C4) cannot be added to the basis without adding previously class C1 (C2) due to the orthogonalization procedure. For example, we cannot add the HH states of class C3 with $K_3 = 6$ without adding previously the HH states of class C1 with $K_1 = 6$. Therefore, to have a clear convergence pattern for class C1 (C2), we studied it without adding class C3 (C4). The changes in the convergence pattern of class C1 (C2) due to the coupling with the class C3 (C4) are in any case negligible, since class C3 (C4) gives a very small contribution to the total binding energy.

In Fig. 1 we plot the values of Δ_1, Δ_2, and Δ_5 for the three SRG evolved potentials considered. By inspecting the figure, we can see a clear exponentially decreasing behavior of the Δ_i as function of K, even if the values of K are rather small. In particular, we can assume for each class that

$$B_i(K) = B_i(\infty) + a_i\, e^{-b_i K}, \quad (34)$$

where $B_i(\infty)$ is the asymptotic binding energy of the class Ci for $K \to \infty$, while a_i and b_i are parameters which depend on the potential and on the class of the HH functions we are studying. In particular, the parameter b_i indicates the convergence rate of the class Ci. From Eq. (34) we obtain

$$\Delta_i(K) = a_i e^{-b_i K}(1 - e^{2b_i}), \quad (35)$$

which is used for fitting $\Delta_i(K)$. The results of the fits are the dashed lines in Figures 1. By observing Figs. 1(a)–1(c) it is clear that the convergence rate diminishes by increasing the values of Λ. We observe also that for $\Lambda = 1.2$ fm^{-1} we have $\Delta_1(K) > \Delta_2(K)$, for $\Lambda = 1.5$ fm^{-1} we have $\Delta_1(K) \approx \Delta_2(K)$, while for $\Lambda = 1.8$ fm^{-1} we have $\Delta_1(K) < \Delta_2(K)$, which confirms the increasing importance of the tensor term of the potential which correlates S and D waves by increasing Λ. Moreover, for all the values of the flow parameter Λ, we find $\Delta_5(K) \ll \Delta_1(K), \Delta_2(K)$, confirming the rapid convergence of the P-waves' contribution to the binding energy. These effects can be seen also by comparing the values of b_i obtained by the fits and reported in Table V. For the classes C3, C4, and C6, the calculated values of $\Delta_i(K)$ are not enough to perform a fit and so we extract the parameter b_i by using only the last two values of Δ_i, namely

$$\frac{\Delta_i(K_{iM} - 2)}{\Delta_i(K_{iM})} = e^{2b_i}. \quad (36)$$

This formula gives only a rough estimate of the convergence rate. The obtained values of b_i are reported in Table V as well. For all the classes the values of b_i decrease when Λ grows, which indicates a more and more repulsive core of the potential when Λ increases.

Before discussing the calculation of the "missing" binding energy, we want to underline that Eq. (35) represents the asymptotic behavior of the convergence pattern when K is large, while we are using value of Δ_i computed for not so large values of K. For this reason, for the final fit of classes

TABLE V. Increments of the ^{6}Li binding energy $\Delta_i(K_{iM})$, computed using Eqs. (28)–(33) for the various classes $i = 1, \ldots, 6$ and the SRG evolved potentials. The coefficients b_i are fitted on the $\Delta_i(K)$ for the classes $i = 1$, 2, and 5 and computed as in Eq. (36) for the classes $i = 3$, 4, and 6. $(\Delta B)_i$ is computed as in Eq. (37) and it represents the "missing" binding energy of each class, due to the truncation of the expansion up to a given K_{iM}. Finally, the "total missing" binding energy $(\Delta B)_T$ is computed from Eq. (39). In parentheses we report the errors. With (0) we indicate that the errors are smaller than the precision of the digits reported in the table.

		SRG1.2			SRG1.5			SRG1.8		
i	K_{iM}	$\Delta_i(K_{iM})$	b_i	$(\Delta B)_i$	$\Delta_i(K_{iM})$	b_i	$(\Delta B)_i$	$\Delta_i(K_{iM})$	b_i	$(\Delta B)_i$
1	14	0.013	0.51	0.007(0)	0.023	0.49	0.014(0)	0.035	0.46	0.023(0)
2	12	0.008	0.68	0.003(1)	0.042	0.58	0.019(0)	0.144	0.50	0.084(11)
3	10	0.015	0.37	0.014(7)	0.022	0.32	0.024(12)	0.024	0.30	0.029(15)
4	10	0.008	0.60	0.004(2)	0.022	0.49	0.013(6)	0.045	0.38	0.039(20)
5	8	0.007	0.52	0.004(0)	0.023	0.37	0.021(0)	0.049	0.26	0.070(1)
6	8	0.004	0.44	0.003(1)	0.018	0.26	0.026(13)	0.048	0.11	0.19(9)
$(\Delta B)_T$				0.034(7)			0.117(19)			0.43(9)

C1 and C2 we used only $\Delta_i(K)$ with $K \geqslant 8$. Indeed, in Fig. 1 it is possible to observe that, for $K \leqslant 6$, Δ_i deviates from the fit. This is usual for the convergence of HH states, as already observed in the case of the α particle in Ref. [21], and is due to the fact that for small values of K the number of states is not enough to give a good description of the wave function.

The "missing" binding energy due to the truncation of the expansion for each class to finite values of $K = K_{iM}$ can be defined as in Ref. [21]:

$$(\Delta B)_i = \sum_{K=K_{iM}+2,K_{iM}+4,\ldots} \Delta_i(K), \tag{37}$$

and, by using Eq. (35), we obtain

$$(\Delta B)_i = \Delta_i(K_{iM}) \frac{1}{e^{2b_i} - 1}. \tag{38}$$

The "total missing" binding energy is then computed as

$$(\Delta B)_T = \sum_{i=1,6} \Delta_i(K_{iM}) \frac{1}{e^{2b_i} - 1}. \tag{39}$$

In Table V we summarize the "missing" binding energy of each class and the "total missing" binding energy. By inspecting the table we observe that the total missing binding energy is less than 1% of the total binding energy for all the SRG evolved potentials. This confirms the high accuracy of the computed binding energies. Regarding the errors on the missing binding energy $[\delta(\Delta B)_i]$, in the case of the classes C1, C2, and C5 we propagate the errors on b_i evaluated in the fits. The estimate of the missing binding energy suffers due to the fact that the extrapolation is not really done for large K, in particular for the classes C3, C4, and C6. Therefore, for these classes we consider a conservative error of $\delta(\Delta B)_i/(\Delta B)_i = 0.5$. The error on the total missing binding energy is then computed as

$$\delta(\Delta B)_T = \sqrt{\sum_{i=1,6} [\delta(\Delta B)_i]^2}. \tag{40}$$

For all the potentials considered, the relative error $\delta(\Delta B)_T/(\Delta B)_T$ is of the order of $\approx$20%.

In Table VI we compare our results with those of Ref. [30], obtained using the NCSM. As can be observed by inspecting columns 1 and 2, the results obtained with the same N3LO500-SRGΛ potentials in Ref. [30] seem to be systematically larger. A possible explanation can be found in the fact that in Ref. [30] the Coulomb potential is included in the SRG evolution. By performing the calculations with the Coulomb interactions included in the SRG evolutions (indicated with IC in Table VI) we gain $\approx$30–40 keV, solving partially the discrepancy. However our results remain still systematically smaller than the ones of Ref. [30], even if for $\Lambda = 1.2$ fm^{-1} and $\Lambda = 1.8$ fm^{-1} they are compatible within the error bars. A possible explanation of the remaining differences could be that we are using a slightly different SRG evolved potential.

C. Electromagnetic static properties

In order to fully characterize the ^{6}Li ground state, we compute the value of charge radius, magnetic dipole moment and electric quadrupole moment. Since the wave function we use is not the "bare" wave function, we should take care of the SRG transformation of the operators in order to be fully consistent. However, it has been argued that long-range operators would not be affected by it [31]. Therefore, in this section we assume that

$$\hat{O} \approx \hat{O}(\Lambda), \tag{41}$$

where $\hat{O}$ is the "bare" operator and $\hat{O}(\Lambda)$ the SRG evolved one. In any case we will verify this approximation by com-

TABLE VI. Values of the computed (B) and extrapolated ($B_{\text{ex.}}$) ^{6}Li binding energy, calculated with the HH basis including (IC) and not including (NIC) the Coulomb interaction in the SRG evolution. Here we report for comparison the extrapolated values of Ref. [30], obtained with the NCSM basis up to $N_{\max} = 10$. All the results are expressed in MeV.

	NIC (HH)		IC (HH)		Ref. [30] (NCSM)
	B	$B_{\text{ex.}}$	B	$B_{\text{ex.}}$	$B_{\text{ex.}}$
SRG1.2	31.75	31.78(1)	31.78	31.81(1)	31.85(5)
SRG1.5	32.75	32.87(2)	32.79	32.91(2)	33.00(5)
SRG1.8	32.21	32.64(9)	32.25	32.68(9)	32.8(1)

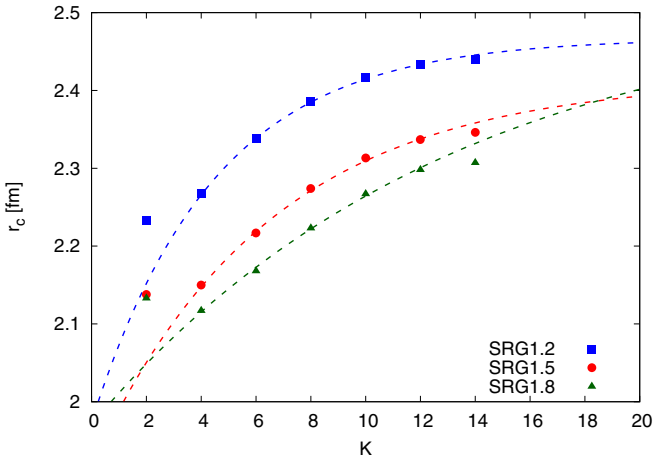

FIG. 2. ^{6}Li charge radius in fm as function of K for the potential models SRG1.2 (blue), SRG1.5 (red), and SRG1.8 (green). The exponential fit performed using Eq. (44) is also shown (dashed lines).

puting the operators for different values of Λ. Moreover, we discuss the convergence of these observables as a function of K. From now on, with K we indicate the fact that for each class we include all the HH states with $K_i \leqslant K$. In the case $K > K_{iM}$ for a given class Ci, we include HH states of this class up to K_{iM}.

1. Charge radius

The mean square (ms) charge radius of a nucleus is given by [32]

$$\langle r_c^2 \rangle = \langle r_p^2 \rangle + \langle R_p^2 \rangle + \frac{N}{Z}\langle R_n^2 \rangle + \frac{3\hbar^2}{2m_p^2 c^2}, \tag{42}$$

where $\langle R_p^2 \rangle$ and $\langle R_n^2 \rangle$ are the ms charge radii of the proton and neutron respectively, and the last term is the Darwin-Foldy relativistic correction [33]. The values used for these three contributions are obtained from Ref. [34]. Moreover, $\langle r_p^2 \rangle$ is the ms value of the proton point radius operator which for the ^{6}Li is defined as

$$\hat{r}_p^2 = \frac{1}{3}\sum_{i=1}^{6} (\boldsymbol{r}_i - \boldsymbol{R}_{\text{c.m.}})^2 \left(\frac{1+\tau_z(i)}{2}\right), \tag{43}$$

where $\boldsymbol{R}_{\text{c.m.}}$ is the c.m. position, $\boldsymbol{r}_i$ the position of the particle i, and 3 the number of protons.

In Figure 2 we plot the values of the root-mean-square charge radius $r_c = \sqrt{\langle r_c^2 \rangle}$ as function of K. From the figure we can observe an exponential behavior as K increases. In order to extrapolate the fully converged value, we fit our results with

$$r_c(K) = r_c(\infty) + ae^{-bK}, \tag{44}$$

where $r_c(\infty)$ is the extrapolated value for $K \to \infty$. The final results are reported in Table VII.

From the fit we have excluded the values of r_c obtained for $K = 2$ and $K = 14$, since they do not follow the exponential behavior, as can be seen in Fig. 2. This is due to the fact that for $K = 2$ there are not enough states to well define the structure of ^{6}Li, and among the states with $K = 14$ we are not considering channels with D states, which are fundamental for describing properly the ^{6}Li radius.

TABLE VII. Extrapolated values for the ^{6}Li charge radii obtained using SRG evolved potentials with $\Lambda = 1.2$, 1.5, and 1.8 fm^{-1}. In the last row we report for comparison the experimental value [35].

	$r_c(\infty)$ (fm)
SRG1.2	2.47(1)
SRG1.5	2.42(2)
SRG1.8	2.52(10)
Expt.	2.540(28)

As can be seen from Fig. 2, the convergence is quite slow. Indeed, the HH basis is a "compact" basis and it is not able to describe perfectly the tail of the wave function, which has an $\alpha + d$ dominant structure. We will treat this point with more details in Sec. IV D. By comparing the results for the various SRG parameters, it is clear that the convergence rate is faster for the smallest values of the parameter Λ, since in these cases the correlations between the nucleons are reduced, favoring the convergence. The approximation of Eq. (41) for this observable is quite reliable since the difference on the extrapolations for the various Λ is less than $\approx$4%.

2. Magnetic dipole moment

The magnetic dipole moment operator for the $A = 6$ case can be written as

$$\hat{\mu}_z = \mu_p \hat{\sigma}_z^p + \mu_n \hat{\sigma}_z^n + \hat{L}_z, \tag{45}$$

where μ_p and μ_n are the proton and neutron intrinsic magnetic moments taken from Ref. [34],

$$\hat{\sigma}_z^{p/n} = \sum_{i=1}^{6} \sigma_z(i) \frac{1 \pm \tau_z(i)}{2} \tag{46}$$

is the total spin of protons and neutrons, and

$$\hat{L}_z^p = \sum_{i=1}^{6} \ell_z(i) \frac{1+\tau_z(i)}{2} \tag{47}$$

is the angular momentum of the protons. The convergence of this operator as function of K does not show an exponential behavior as in the charge radius case, but is quite fast since it depends only on the percentage of the various partial waves, which are very stable, being integral quantities. In Table VIII we report the mean values of the magnetic dipole moment obtained in the full configuration at $K = 14$. Since we cannot give a reliable extrapolation to $K \to \infty$, as we have done for the charge radius, we consider a conservative theoretical error defined as

$$\Delta\mu_z = \max_{K=8,10,12} \{|\mu_z(K) - \mu_z(14)|\}, \tag{48}$$

where $\mu_z(K)$ is the value of the dipole magnetic moment of the ^{6}Li wave function computed using K as the maximum value for the grand-angular momentum.

TABLE VIII. Values of the magnetic dipole moment μ_z for ^{6}Li evaluated using SRG evolved potential models with $\Lambda = 1.2$, 1.5, and 1.8 fm^{-1}. We report also the value of the magnetic dipole moment of the deuteron $\mu_z(d)$ computed with the same potentials. In the last row the experimental values are listed [36].

	$\mu_z(^6\text{Li})$ (μ_N)	$\mu_z(d)$ (μ_N)
SRG1.2	0.865(1)	0.872
SRG1.5	0.858(2)	0.868
SRG1.8	0.852(2)	0.865
Expt.	0.822	0.857

TABLE IX. Values of the ^{6}Li electric quadrupole moment obtained for SRG evolved potential models with $\Lambda = 1.2$, 1.5, and 1.8 fm^{-1}. In the last row we report for comparison the experimental value [36].

	Q ($e$fm^2)
SRG1.2	−0.191(7)
SRG1.5	−0.101(7)
SRG1.8	−0.055(3)
Expt.	−0.0806(6)

As it can be seen by inspecting the table, the value of the magnetic dipole moment slightly decreases by increasing the value of Λ. Indeed, when Λ increases the correlations induced by the nuclear potential are stronger, generating a larger amount of D component in the wave function, which reduces the value of μ_z. However, the differences between the various Λ are ≈1%, confirming that Eq. (41) is a quite good approximation for this observable.

If we consider ^{6}Li to be formed as a $\alpha + d$ cluster, we can expect that

$$\mu_z(^6\text{Li}) \approx \mu_z(d), \tag{49}$$

because the α particle has no magnetic dipole moment. However, the internal structure of ^{6}Li plays a fundamental role in decreasing the value of the magnetic dipole moment compared to the deuteron one, as can be observed by comparing the experimental values (last row of Table VIII). In Table VIII we compare the results of the magnetic dipole moment of ^{6}Li and d computed with the same SRG potentials. In all the cases, the ^{6}Li magnetic dipole moment is reduced compared to the d ones, showing that the potential models are going in the right direction, even if they are not able to reproduce the experimental value. Obviously this is partially due to the fact we are not considering the evolved operator and also that we are not including three-body forces. Moreover, as shown in Refs. [37,38] for ^{3}H and ^{3}He, the magnetic dipole moment receives important contributions from two-body electromagnetic currents. Therefore, we can expect that similar corrections are necessary in this case to reproduce the experimental value of $\mu_z(^6\text{Li})$.

3. Electric quadrupole moment

The electric quadrupole moment operator for $A = 6$ is defined as

$$\hat{Q} = \sum_{i=1}^{6} \left(3z_i^2 - r_i^2\right)\left(\frac{1+\tau_z(i)}{2}\right). \tag{50}$$

The study of this observable is crucial for understanding the goodness of the ^{6}Li wave function we computed. Indeed, from the experiment, we know that the electric quadrupole moment of ^{6}Li is very small and negative. For this reason, it is challenging for all the potential models to reproduce this value.

The convergence of this operator as function of K shows an irregular trend due to large cancellations among the contributions coming from different sets of HH states. Therefore, as for the magnetic dipole moment, we report in Table IX the value of this operator obtained for $K = 14$ and the errors computed as given in Eq. (48), substituting the dipole magnetic moment with the electric quadrupole moment. The values obtained for the SRG potentials are quite dependent on the value of the parameter Λ. Therefore, for the electric quadrupole moment the approximation of Eq. (41) seems not to be valid. However, all the considered SRG evolved potentials are able to reproduce a small and negative value for the electric quadrupole moment. In particular, for $\Lambda = 1.5$ and 1.8 fm^{-1}, we obtain values quite close to the experimental value of −0.0806(6) e fm.

In order to understand why we have these differences between the various SRG evolved potentials, we report in Table X the partial wave contributions to this observable. As can be seen, we have large differences only in the contribution coming from matrix element between S and D waves. In particular the value of this matrix element increases when Λ increases. Therefore, the value of the electric quadrupole moment seems directly connected to the strength of the tensor term in the nuclear potential. Indeed, we can expect that if the correlations between S and D waves grow (as in the case of "bare" chiral potentials), the value of the electric quadrupole moment could come positive. Therefore, also in this case, the two-body current corrections to this observable could be necessary to explain the observed value of ^{6}Li electric quadrupole moment.

D. Asymptotic normalization coefficients

The asymptotic normalization coefficients (ANCs) are properties of the bound state wave functions that can be

TABLE X. Partial wave contributions to the ^{6}Li electric quadrupole moment obtained using SRG evolved potentials with $\Lambda = 1.2$, 1.5, and 1.8 fm^{-1}. All the values are given in unit of e fm^2.

	S-D	*D-D*	*P-P*	*P-D*	Remaining
SRG1.2	−0.187	−0.023	0.009	0.009	<0.001
SRG1.5	−0.102	−0.023	0.014	0.010	<0.001
SRG1.8	−0.058	−0.024	0.016	0.010	0.001

related to experimental observables. In particular, in the case of the $\alpha + d$ radiative capture, it plays a fundamental role in the determination of the cross section. Moreover, the ANCs provide a test of quality of the variational wave function in the asymptotic region where the 4+2 clusterization is dominant.

In the asymptotic region, where the ^{6}Li is clustered, the ^{6}Li wave function is

$$\Psi_{^6\mathrm{Li}} \to C_0 \frac{W_{-\eta,1/2}(2kr)}{r} \Psi^{(0)}_{\alpha+d} + C_2 \frac{W_{-\eta,5/2}(2kr)}{r} \Psi^{(2)}_{\alpha+d}. \quad (51)$$

The function $\Psi^{(L)}_{\alpha+d}$ is the $\alpha + d$ cluster wave function, which is defined as

$$\Psi^{(L)}_{\alpha+d} = \frac{1}{\sqrt{15}} \mathcal{A}[(\Psi_\alpha \times \Psi_d)_1 Y_L(\hat{r})]_1, \quad (52)$$

where the symbol $\mathcal{A}$ is the antisymmetrization operator, Ψ_α and Ψ_d are the wave functions of the α particle and the deuteron calculated in the HH variational approach, and $\boldsymbol{r}$ is the distance between the c.m. of the α particle and the deuteron. In the previous equation, the spin 0 of the α particle is combined with spin 1 of the deuteron giving a "channel" spin $S = 1$. The channel spin is then coupled with the angular momentum L to give a total angular momentum $J = 1$. Because of the even parity of ^{6}Li, α, and d, the $\alpha + d$ cluster can be only in states $L = 0, 2$. In Eq. (51), $W_{-\eta,L+1/2}(2kr)$ is the Whittaker function with k and η determined as

$$k = \sqrt{\frac{8}{3}\frac{m}{\hbar^2}B_c}, \qquad \eta = \frac{3}{4}\frac{m}{\hbar^2}\frac{e^2}{k}. \quad (53)$$

Here we have used $e^2 = 1.44$ MeV fm, $\hbar^2/m = 41.47$ MeV fm^2, and $B_c = B_{^6\mathrm{Li}} - B_\alpha - B_d$ with $B_{^6\mathrm{Li}}$, B_α, and B_d the ^{6}Li, α, and d binding energies, respectively. Finally, $C_{0/2}$ of Eq. (51) are the $L = 0$ and $L = 2$ ANCs, respectively.

In order to compute C_L, we have defined the $\alpha + d$ overlap as

$$f_L(r) = r \frac{\langle \Psi_{^6\mathrm{Li}} | \Psi^{(L)}_{\alpha+d} \rangle_r}{[\langle \Psi_d|\Psi_d\rangle\langle\Psi_\alpha|\Psi_\alpha\rangle\langle\Psi_{^6\mathrm{Li}}|\Psi_{^6\mathrm{Li}}\rangle]^{1/2}}, \quad (54)$$

where we have defined the proper norms of a generic wave function of A bodies as

$$\langle \Psi_A|\Psi_A\rangle = \int \prod_{i=1}^{A} d\boldsymbol{r}_i \, \delta\left(\boldsymbol{R}^A_{\mathrm{c.m.}} - \frac{1}{A}\sum_{j=1}^{A}\boldsymbol{r}_j\right) |\Psi_A|^2 = 1, \quad (55)$$

and $\boldsymbol{R}^A_{\mathrm{c.m.}}$ is the generic position of the c.m. of the A particles. Moreover, in Eq. (54) we indicate with $\langle\rangle_r$ the fact that we are performing the spin-isospin traces and the integration over all the positions of the particles except the intercluster distance r and the center of mass. With such definition the overlap is completely independent of the choice of the internal variables. To perform the calculation it is convenient to introduce the proper set of Jacobi coordinates (set "B") to describe the $\alpha + d$ clusterization, defined as

$$\begin{aligned}
\boldsymbol{\xi}_{1Bp} &= \boldsymbol{r}_n - \boldsymbol{r}_m, \\
\boldsymbol{\xi}_{2Bp} &= \sqrt{\frac{8}{3}}\left(\frac{\boldsymbol{r}_n + \boldsymbol{r}_m}{2} - \frac{\boldsymbol{r}_l + \boldsymbol{r}_k + \boldsymbol{r}_j + \boldsymbol{r}_i}{4}\right), \\
\boldsymbol{\xi}_{3Bp} &= \sqrt{\frac{3}{2}}\left(\boldsymbol{r}_l - \frac{\boldsymbol{r}_k + \boldsymbol{r}_j + \boldsymbol{r}_i}{3}\right), \\
\boldsymbol{\xi}_{4Bp} &= \sqrt{\frac{4}{3}}\left(\boldsymbol{r}_k - \frac{\boldsymbol{r}_j + \boldsymbol{r}_i}{2}\right), \\
\boldsymbol{\xi}_{5Bp} &= \boldsymbol{r}_j - \boldsymbol{r}_i.
\end{aligned} \quad (56)$$

Then, the overlap function reduces to

$$\begin{aligned}
f_L(r) = r\sqrt{15}\left(\frac{\sqrt{6}}{4}\right)^{\frac{3}{2}} \int \prod_{i=1}^{5} d\boldsymbol{\xi}_{iB} \, \delta\left(r - \sqrt{\frac{3}{8}}\xi_{2B}\right) \\
\times \Psi_{^6\mathrm{Li}}(\boldsymbol{\xi}_{1B}, \boldsymbol{\xi}_{2B}, \boldsymbol{\xi}_{3B}, \boldsymbol{\xi}_{4B}, \boldsymbol{\xi}_{5B}, \boldsymbol{\xi}_{6B})^\dagger \\
\times \left[(\Psi_\alpha(\boldsymbol{\xi}_{3B}, \boldsymbol{\xi}_{4B}, \boldsymbol{\xi}_{5B}) \times \Psi_d(\boldsymbol{\xi}_{1B}))_1 Y_L(\hat{r})\right]_1,
\end{aligned} \quad (57)$$

where we have used the antisymmetry of the ^{6}Li wave function to eliminate the antisymmetrization operator $\mathcal{A}$, and we have multiplied by a factor 15 to take care of the fact that the initial function $\Psi^{(L)}_{\alpha+d}$ contains that number of $4 + 2$ partitions of the six particles. Finally, $(\sqrt{6}/4)^{\frac{3}{2}}$ is a factor that comes from the normalizations of the wave functions. In Eq. (57) we indicate with $\Psi_\alpha(\boldsymbol{\xi}_{3B}, \boldsymbol{\xi}_{4B}, \boldsymbol{\xi}_{5B})$ the wave function of the α particle constructed as the sum over the 12 even permutations of the particles (1,2,3,4) and with $\Psi_d(\boldsymbol{\xi}_{1B})$ the wave function of the deuteron constructed with the particles (5,6). The ^{6}Li wave function is the one of Eq. (24) rewritten in terms of the set "B" of Jacobi coordinates, by redefining properly the TCs. The ANCs is then obtained by

$$C_L = \lim_{r\to\infty} C_L(r), \quad (58)$$

where

$$C_L(r) = \frac{f_L(r)}{W_{-\eta,L+1/2}(2kr)}. \quad (59)$$

The dependence of the overlap to the truncation level of the HH expansion of ^{6}Li is studied by varying the maximum value of K. In Fig. 3 we plot the $L = 0$ component of the overlap function obtained with the SRG1.5 potential. From the figure it is clear that the tail of the overlap does not have the correct behavior of the Whittaker function (full red line). This is due to the limited number of HH states used in the expansion of the ^{6}Li wave function, which is not enough to reproduce the correct asymptotic behavior. However, it is also clear that the HH states are slowly constructing the correct asymptotic slope when K increases. In reverse, for the short-range part ($r < 3$ fm) the convergence is fast and completely reached. Similar comments apply also for all the other potentials and the $L = 2$ component. The results obtained for the $L = 0$ and $L = 2$ overlaps are qualitatively consistent with the ones reported in Refs. [39–42].

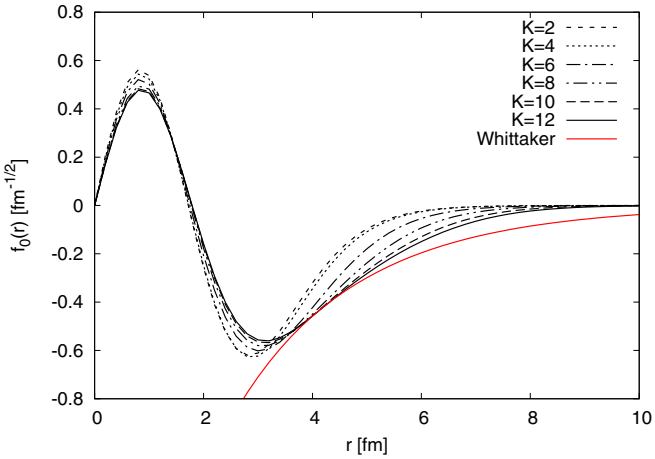

FIG. 3. S-wave component of the overlap function $f_L(r)$ defined in Eq. (57) for different values of K used in the expansion of the ^{6}Li wave function. The full red line represents the correct asymptotic behavior given by the Whittaker function. These results are obtained with the SRG1.5 potential.

By using Eq. (59), we can then calculate the ANCs. In Figs. 4 and 5 we illustrate with the dashed lines the ratios $C_0(r)$ and $C_2(r)$ computed in the SRG1.5 case, for $K = 10$ (blue) and $K = 12$ (red). Both the functions $C_0(r)$ and $C_2(r)$ show a sort of "plateau" around the minimum (maximum in the case of $L = 2$), from which we can have a crude estimate of the ANC. We observe the same behavior for all the other potentials considered in this paper. In Table XI with Method I we indicate the estimate of the ANCs for both $L = 0$ and $L = 2$ components and the various SRG evolved potentials obtained with this approach. The numerical differences among the ANCs obtained from the three potentials are mostly due to the different values of k, present in η [see Eq. (53)], entering in the Whittaker function. The values of B_c, from which the value of k depends, are reported as well in Table XI.

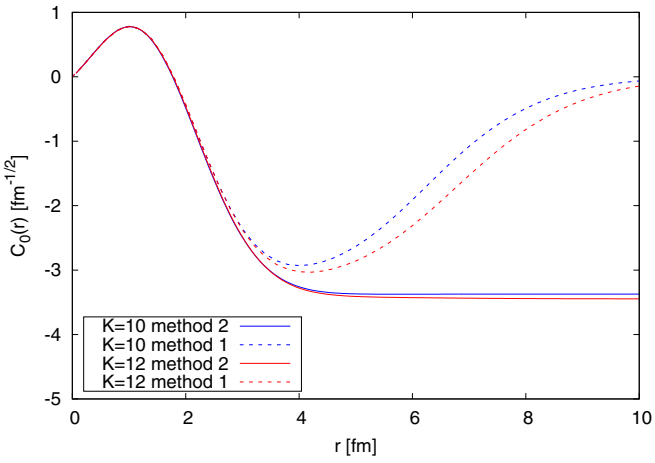

FIG. 4. Function $C_0(r)$ computed with the overlap method (dashed lines) and the equation method (continuous lines) for the SRG1.5 potential. The calculations are performed with the ^{6}Li wave function computed with $K = 10$ (blue lines) and $K = 12$ (red lines). Results of the equation method are obtained using $\overline{K} = 8$.

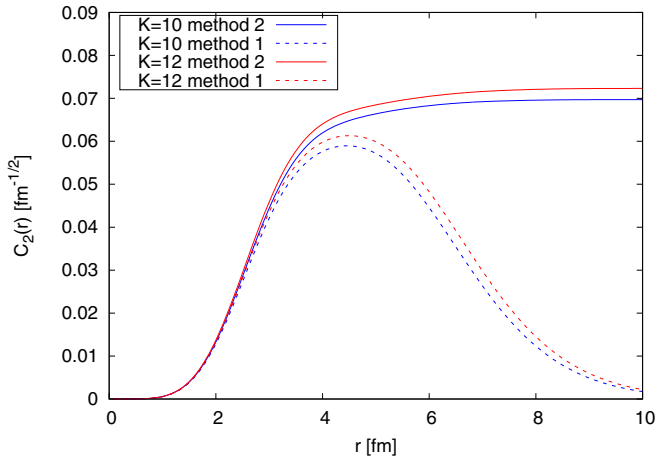

FIG. 5. The same as Figure 4, but for the function $C_2(r)$.

From the overlap it is also possible to compute the spectroscopic factor $\mathcal{S}_L$ defined as

$$\mathcal{S}_L = \int_0^\infty dr\, f_L(r)^2, \tag{60}$$

which can be interpreted as the percentage of $\alpha + d$ clusterization in the ^{6}Li wave function. In Table XII we report the values of the spectroscopic factors obtained for the various potentials. Independently of the Λ parameter used, the $\alpha + d$ clusterization represents more than 80% of the ^{6}Li wave function. The differences between the values obtained with the SRG evolved potentials can be due to the fact that the induced and proper three-body forces are not included. Moreover, in the table we compare our results with the calculation of Refs. [39–41]. The values are similar, even if obtained with different potential models, and compatible with the experimental estimate of Ref. [46].

Since the procedure adopted so far for extrapolating the ANCs is somewhat unsatisfactory, due to the difficult identification of the "plateau," we use another procedure, based on Ref. [48] and already applied in Ref. [21]. With this approach, we can extrapolate the ANCs with greater accuracy. Assuming that Ψ_α and Ψ_d are "exact," it is not difficult to show that the overlap function $f_L(r)$ should satisfy the equation

$$\left[-\frac{\hbar^2}{2\mu}\left(\frac{d^2}{dr^2} - \frac{L(L+1)}{r^2}\right) + \frac{2e^2}{r} + B_c\right] f_L(r) + g_L(r) = 0, \tag{61}$$

where $\mu = 4/3m$ is the reduced mass of the $\alpha + d$ system, and

$$g_L(r) = r\sqrt{15}\left(\frac{\sqrt{6}}{4}\right)^{\frac{3}{2}} \int \prod_{i=1}^{5} d\boldsymbol{\xi}_{iB}\, \delta\left(r - \sqrt{\frac{8}{3}}\xi_{2B}\right) \times \Psi_{^6\mathrm{Li}}(\boldsymbol{\xi}_{1B}, \ldots, \boldsymbol{\xi}_{5B})^\dagger \left(\sum_{i\in\alpha}\sum_{j\in d} V_{ij} - \frac{2e^2}{r}\right) \times [(\Psi_\alpha(\boldsymbol{\xi}_{3B}, \boldsymbol{\xi}_{4B}, \boldsymbol{\xi}_{5B}) \times \Psi_d(\boldsymbol{\xi}_{1B}))_1 Y_L(\hat{r})]_1, \tag{62}$$

TABLE XI. Values of the ANC C_0 and C_2 in fm$^{-1/2}$ for the various SRG evolved potentials with $\Lambda = 1.2$, 1.5, and 1.8 fm^{-1} and the two methods used for their calculation. We report also the binding energy B_c (MeV) used in the calculation of the ANC and the ratio C_2/C_0. For completeness, we show also the results of the *ab initio* calculation of Refs. [43,44] obtained with an SRG evolved potential with $\Lambda = 2.0$ fm^{-1} (SRG2.0) derived from the same two-nucleon force as in the present work, considering only two-body forces (NN) and three-body forces (3b) respectively, and the results of Ref. [40] obtained with AV18/UIX potential. Also the experimental values of Ref. [45] are listed.

	Model	B_c (MeV)	C_0 (fm$^{-1/2}$)	C_2 (fm$^{-1/2}$)	C_2/C_0
	SRG1.2	3.00(1)	−3.9	0.10	−0.03
Method 1	SRG1.5	2.46(2)	−3.0	0.06	−0.02
	SRG1.8	2.01(9)	−2.3	0.03	−0.01
	SRG1.2	3.00(1)	−4.19(12)	0.116(18)	−0.028(5)
Method 2	SRG1.5	2.46(2)	−3.44(7)	0.072(15)	−0.021(5)
	SRG1.8	2.01(9)	−3.01(7)	0.047(10)	−0.016(4)
Ref. [43]	SRG2.0(NN)	1.52	−2.63	0.031	−0.012
Ref. [44]	SRG2.0(3b)	1.49	−2.695	0.074	−0.027
Ref. [40]	AV18/UIX	1.47	−2.26(5)		−0.027(1)
Ref. [45]	Expt.	1.4743	−2.91(9)	0.077(18)	−0.025(11)

is the so called source term with V_{ij} the two-body potential. As $r \to \infty$, the function $g_L(r) \to 0$, and the solution of Eq. (61) coincides with the Whittaker function, allowing for the extraction of the ANC using Eq. (58). Since the calculation of $g_L(r)$ in this form is quite involved, we expand the cluster part $[(\Psi_\alpha \times \Psi_d)_1 Y_L(\hat{r})]_1$ for a given permutation p in terms of HH functions, i.e.,

$$[(\Psi_\alpha \times \Psi_d)_1 Y_L(\hat{r})]_1 F(r) = \sum_{[\overline{K}],\bar{l}} c_{[\overline{K}],\bar{l}} \Phi_{[\overline{K}]}(i,j,k,l,m,n) f_{\bar{l}}(\rho), \quad (63)$$

where $c_{[\overline{K}],\bar{l}}$ are the parameters of the expansion, $\Phi_{[\overline{K}]}(i,j,k,l,m,n)$ are the HH states defined in Eq. (13), $f_{\bar{l}}(\rho)$ are the hyperradial functions of Eq. (25), and with $[\overline{K}], \bar{l}$ we indicate the full set of quantum numbers. $F(r)$ is an intercluster function constructed by rearranging Eq. (62). The expansion is then controlled by the parameters $\overline{K}$ and $\bar{l}$. We obtain full convergence on the hyperradius with $\bar{l} = 40$, while the convergence as function of $\overline{K}$ is discussed in detail in the following. By replacing the cluster part with the HH expansion, the source term reduces to products of the coefficients $c_{[\overline{K}],\bar{l}}$ and matrix elements of the potential between HH states, already calculated as described in Appendix A. More details on the calculation of the source term can be found in Appendix B.

In Figure 6 we plot the source term $g_L(r)$ for the $L = 0$ component in the case of the SRG1.5 potential for different values of $\overline{K}$. The calculation shown in this plot is performed by considering the ^{6}Li wave function computed for $K = 12$. From the figure it is immediately clear that we have a nice convergence in $\overline{K}$ for the short-range part ($r < 3$–4 fm) but not for larger r. This effect is due to the fact that the Jacobi polynomials are not flexible enough in reproducing the exponential behavior of the cluster wave functions of Eq. (B5). However, by inspecting the figure, it is clear that there are problems only in a region where $g_0(r)$ is a factor 100 smaller than the peak. A similar convergence behavior in $\overline{K}$ is found also for the other potentials studied and for $g_2(r)$.

TABLE XII. Values of the spectroscopic factors for the various SRG-evolved potentials with $\Lambda = 1.2$, 1.5, and 1.8 fm^{-1}. In the last rows we compare our results with the results obtained within the GFMC using the AV18/UIX interaction, the result obtained within the NCSM using a unitary transformed version of the CD-Bonn2000 (CD-B2k) potential [47], and the experimental one.

Method	Potential	$\mathcal{S}_0$	$\mathcal{S}_2$	$\mathcal{S}_0 + \mathcal{S}_2$
HH (This work)	SRG1.2	0.909	0.008	0.917
	SRG1.5	0.868	0.007	0.875
	SRG1.8	0.840	0.006	0.846
GFMC (Ref. [39])	AV18/UIX	0.82	0.021	0.84
GFMC (Ref. [40])	AV18/UIX			0.87(5)
NCSM (Ref. [41])	CD-B2k	0.822	0.006	0.828
Expt. (Ref. [46])				0.85(4)

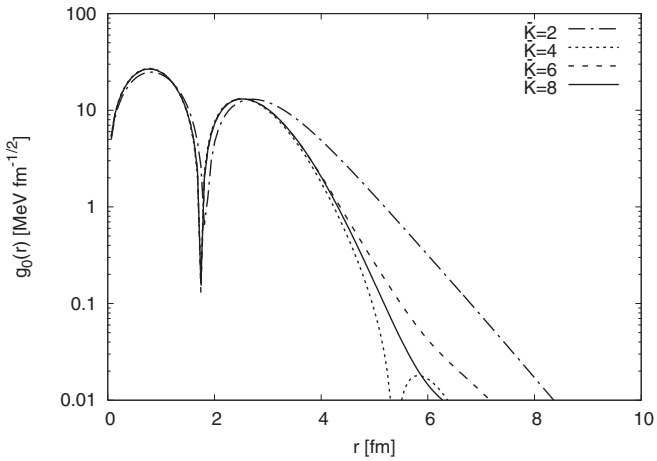

FIG. 6. The source term $g_0(r)$ for different values of $\overline{K}$ used in the projection of the $\alpha + d$ cluster wave functions. This figure is obtained by using SRG1.5 potential and the ^{6}Li wave function computed with $K = 12$.

These considerations on $g_L(r)$ reflect directly on the calculated overlap via Eq. (61). Indeed, thanks to the fact that the term $g_L(r)$ vanishes for large r, we obtain the correct asymptotic behavior, namely the Whittaker function. In Figs. 4 and 5 we compare the functions $C_0(r)$ and $C_2(r)$ obtained by solving the equation (full lines) with the ones obtained from the overlap (dashed lines). In the figures we report the results obtained for SRG1.5 where we used values of $K = 10$ and 12 for the calculation of the ^{6}Li wave function and $\overline{K} = 8$ for the expansion of the cluster wave function. From Figs. 4 and 5 it is clear that in the short-range part ($r < 2$–3 fm) the two approaches are essentially indistinguishable, proving the validity of our expansion of the cluster wave function in HH states. For larger r the two approaches start to diverge since the functions $C_0(r)$ and $C_2(r)$ computed with the direct overlap are not following the correct asymptotic behavior, as already discussed. Similar results are obtained also for the other two SRG evolved potentials. We observe that the "harder" the potential is, the smaller is the value of r for which the disagreement between the two approaches starts to be important. This is an evidence of the fact that also the convergence in $\overline{K}$ depends on the potential.

From the equation method it is easy now to determine the ANCs with great accuracy as function of K and $\overline{K}$ [$C_L(K, \overline{K})$]. As function of $\overline{K}$ the ANCs do not have a smooth convergence and this does not permit us to give a reliable extrapolation for $\overline{K} \to \infty$. Therefore, we consider as best values the ANCs obtained at $\overline{K} = 8$, to which we add a conservative error of

$$\Delta C_L^{(0)}(K) = 0.5 \times |C_L(K, \overline{K} = 6) - C_L(K, \overline{K} = 8)|. \quad (64)$$

Regarding the expansion in K, the convergence is smooth and shows a clear exponential behavior. Therefore we fit the values $C_L(K, 8)$ using

$$C_L(K, 8) = C_L(\infty, 8) + ae^{-bK}. \quad (65)$$

Also for this expansion we consider a conservative error of

$$\Delta C_L^{(1)} = 0.5 \times |C_L(12, 8) - C_L(\infty, 8)|. \quad (66)$$

The total error on the final value $C_L(\infty, 8)$ is

$$\Delta C_L = \sqrt{\left(\Delta C_L^{(0)}(12)\right)^2 + \left(\Delta C_L^{(1)}\right)^2}. \quad (67)$$

In Table XI with Method II we indicate our final results for $C_L(\infty, 8)$. Also in this case the numerical differences among the ANCs for the three SRG-evolved potentials are due to the different binding energies B_c used to compute the Whittaker functions. From the table it is also evident that the results obtained with the equation method are systematically larger than the one estimated by the overlap itself. Even if the results obtained with the equation are affected by significant errors due to the expansion in the HH states of the cluster wave functions, we consider these to be more reliable. Indeed, those obtained from the overlap suffer from the difficulty of individuating unambiguously a well-defined plateau and therefore there might be unknown systematical error. For completeness in the table we report also the experimental values of Ref. [45], the calculation of Ref. [40] obtained with the Argonne v_{18} (AV18) NN interaction [49] combined with the Urbana IX (UIX) three-nucleon potential [50], and the results of Refs. [43,44] obtained with an SRG evolved potential, derived using $\Lambda = 2.0$ fm^{-1} and the same two-nucleon interaction of Ref. [27] as in our case, without or with three-body forces, respectively. We cannot really perform a comparison with the results of Refs. [40,44], since our results do not contain the contribution of the three-body forces, even if, from a qualitative point of view, the results are quite satisfactory. On the other hand, we can compare directly our values with the results of Ref. [43]. Indeed, the results given in Ref. [43] are in line with the trend of the ANCs as function of Λ, as we observe in Table XI for the values obtained with the equation method. This confirms the validty of the equation approach used in computing the ANCs.

V. THE ROLE OF ^{6}Li IN THE DIRECT DARK MATTER SEARCH

In recent years experiments devoted to the direct search for dark matter have planned to use light nuclei, and in particular lithium, as probes to search for signals of light spin-dependent dark matter [51]. Usually, in the determination of the sensitivity limit, very old shell-model calculations for nuclei are considered. However, it is very well known that all shell models fail to describe the ^{6}Li structure. The aim of this section is to furnish a reliable calculation of the necessary matrix elements.

The formula that is usually used to determine the rate of events for spin-dependent dark matter is proportional to $\langle S_{p/n}\rangle^2$ [52], where $\langle S_{p/n}\rangle$ is the mean value of the proton (neutron) spin operator

$$\hat{S}_{p/n} = \frac{1}{2}\sum_{i=1}^{6} \sigma(i)\frac{1 \pm \tau_z(i)}{2} \quad (68)$$

on the nuclear wave function. In the case of ^{6}Li, if we consider it as a pure state of isospin $T = 0$, by exploiting Wigner-Eckart theorem, it is easy to show that

$$\langle S_p\rangle_{^6\mathrm{Li}} = \langle S_n\rangle_{^6\mathrm{Li}}. \quad (69)$$

In order to give a very rough estimate of these matrix elements for ^{6}Li, we can consider it as an $\alpha + d$ cluster. If we suppose that α is a fully spin-0 particle, the only contribution to the spin of ^{6}Li comes from the deuteron, namely

$$\langle S_p\rangle_{^6\mathrm{Li}} = \langle S_n\rangle_{^6\mathrm{Li}} \approx 0.5. \quad (70)$$

In our calculation we considered the full ^{6}Li structure. In particular, by taking care of all the possible partial waves which compose the ^{6}Li wave function, the spin operator is

$$\langle S_{p/n}\rangle_{^6\mathrm{Li}} = \tfrac{1}{2}P_{^3S_1} + \tfrac{1}{4}P_{^1P_1} + \tfrac{3}{4}P_{^3P_1} - \tfrac{1}{4}P_{^3D_1} + \tfrac{1}{4}P_{^5D_1} + P_{^7D_1} - \tfrac{1}{2}P_{^5F_1} + \tfrac{1}{4}P_{^7F_1} - \tfrac{3}{4}P_{^7G_1}, \quad (71)$$

where P_i is the percentage of the i wave in the ^{6}Li wave function. In Table XIII we present the results obtained for the proton (neutron) spin with the three different SRG evolved potentials used in this work. The errors are computed as in Eq. (48) by substituting the magnetic dipole moment with the spin operator. The differences among the three values and the result of Eq. (70) are directly related to the presence of

TABLE XIII. Mean values of the proton (neutron) spin operator obtained using SRG evolved potentials with $\Lambda = 1.2$, 1.5, and 1.8 fm^{-1}.

	$\langle S_p \rangle$ $(= \langle S_n \rangle)$
SRG1.2	0.479(1)
SRG1.5	0.472(2)
SRG1.8	0.464(3)

D-wave components in ^{6}Li. Indeed, the larger the D-wave components are (and in particular the $^3D_1$), the smaller is the value of the spin operator. It is worthwhile to mention that also for this observable the contribution of two-body currents could be important (see for example Ref. [53] for a detailed discussion on this for the spinless dark matter case).

VI. CONCLUSIONS AND PERSPECTIVES

We have studied the solution of the Schrödinger equation for the six-nucleon ground state using the HH functions. The main problem in using the HH approach is the large degeneracy of the basis. Therefore, we performed a selection of the HH states that gives the most important contributions by following the same procedure used in Ref. [21] for the α-particle ground state. The selection was performed by dividing the HH functions into classes depending on their total angular momentum and spin, as well as other quantum numbers. For each class we truncate the expansion so as to obtain the required accuracy.

Many modern NN potentials contain a strong repulsive core which makes it impossible to reach adequate accuracy with variational approaches in $A = 6$ systems, because of the huge number of states needed in the wave function expansion. Therefore, in this work we limited our study to the N3LO500 chiral interaction of Ref. [27] evolved with the SRG unitary transformation. This permits us to reach good accuracy with the HH available basis. In this first study we considered only two-body forces, even if the HH formalism is versatile enough to treat also three-body interactions without any additional problem. The inclusion of three-nucleon forces is currently in progress.

We have performed the calculation of the binding energy and of electromagnetic properties of ^{6}Li. Since we are not considering three-body forces, neither proper nor induced by the SRG evolution, a meaningful comparison of our results with the experimental values is still premature. Regarding the electromagnetic properties of ^{6}Li, we have observed a strong dependence on the strength of the tensor forces. In future, we plan to include also the effect of two-body currents, necessary probably to explain the small and negative electric quadrupole moment of ^{6}Li. Finally, we have studied the $\alpha + d$ clusterization with the goal of determining the asymptotic normalization coefficients. In doing this, we performed a projection of the cluster wave function on the HH states. This approach can be used also in the study of scattering states, in order to simplify the calculation of the potential matrix elements. The calculation of the $\alpha + d$ scattering within this approach is also in progress.

This work was motivated in order to reach three goals. The first one is to show that the HH expansion applied to the six-nucleon bound problem can reach the same level of precision as other approaches, such as the NCSM, by using the same potentials. In this sense this work represents an important benchmark for both the HH and the NCSM techniques in the $A = 6$ system. The second goal is the extension of this approach to work with "bare" chiral interactions also in the case of the six-nucleon problem. All the results reported here were obtained by working on a single core with few tens of CPUs. Therefore, we expect that it is possible to consider a larger basis by using more massive parallelization. We hope this will allow us to reach a good accuracy also with a "bare" chiral interaction. Moreover, the selection of the classes can be improved, reducing the number of states needed in the expansion. The third goal will be the possibility of using this algorithm for systems up to $A = 8$. Also in this case a massive parallelization will be fundamental. However, also other approaches directly inspired by the NCSM method, such as the inclusion of a clustered component in the wave function, can be implemented in the HH formalism in order to improve the convergence.

ACKNOWLEDGMENTS

A.G. wish to thanks P. Navrátil for a useful discussion on NCSM results for ^{6}Li. Computations were performed on the MARCONI supercomputer at CINECA in Bologna.

APPENDIX A: MATRIX ELEMENTS OF TWO-BODY FORCES

The biggest computational challenge for applying the HH formalism to the $A = 6$ system is the calculation and the storage of the potential matrix elements, because of the high number of basis states needed to reach convergence. In this Appendix we present some details of calculation of the NN potential matrix elements in the HH formalism and also the main features of the algorithm that we implemented to compute the potential matrix elements, exploiting the advantages of using the TCs.

1. Explicit calculation

In the HH method for the $A = 6$ case the matrix element of the NN potential can be written as

$$V^{KLST,K'L'S'T',J\pi}_{l\alpha,l'\alpha'} = 15\langle f_l \Psi^{KLSTJ\pi}_{\alpha} | V_{12} | f_{l'} \Psi^{K'L'S'T'J\pi}_{\alpha'} \rangle_{\Omega,\rho}, \tag{A1}$$

where $\Psi^{KLSTJ\pi}_{\alpha}$ is defined in Eq. (12), f_l is defined in Eq. (25), and $\langle\rangle_{\Omega,\rho}$ denotes the spin and isospin traces and the integration over the hyperspherical and hyperradial variables. The factor 15 takes into account the number of possible pairs in $A = 6$ systems.

In order to compute this matrix element it is convenient to use the jj-coupling scheme in which the basis state α is

$$\Psi_{\alpha}^{KLSTJ\pi} = \sum_{\nu} B_{\alpha,\nu}^{KLSTJ\pi}\ \Xi_{\nu}^{KTJ\pi}(1,2,3,4,5,6), \tag{A2}$$

where the new transition coefficients $B_{\alpha,\nu}^{KLSTJ\pi}$ are connected to the coefficients $A_{\alpha,\alpha'}^{KLSTJ\pi}$ via $6j$- and $9j$-Wigner coefficients. The explicit expression for $\Xi_{\nu}^{KTJ\pi}(1,2,3,4,5,6)$ is given by

$$\begin{aligned}\Xi_{\nu}^{KTJ\pi}(1,\ldots,6) = \mathcal{P}_{n_2,n_3,n_4,n_5}^{\ell_1,\ell_2,\ell_3,\ell_4,\ell_5}(\varphi_2,\varphi_3,\varphi_4,\varphi_5)\Big\{\Big[\big(Y_{\ell_5}(\hat{\xi}_5)(s_1s_2)_{S_2}\big)_{j_1}\big(Y_{\ell_4}(\hat{\xi}_4)s_3\big)_{j_2}\Big]_{j_{12}}\Big[\Big\{\big(Y_{\ell_1}(\hat{\xi}_1)\\ \times Y_{\ell_2}(\hat{\xi}_2)\big)_{L_2}Y_{\ell_3}(\hat{\xi}_3)\Big\}_{L_3}\big((s_4s_5)_{S_4}s_6\big)_{S_5}\Big]_{j_3}\Big\}_{JJ_z}\Big[\big((t_1t_2)_{T_2}t_3\big)_{T_3}\big((t_4t_5)_{T_4}t_6\big)_{T_5}\Big]_{T,T_z}.\end{aligned} \tag{A3}$$

The index ν labels all possible choices of the quantum numbers,

$$\nu \equiv \{n_5,\ell_5,S_2,j_1,n_4,\ell_4,j_2,j_{12},\ell_1,\ell_2,\ell_3,L_2,L_3,n_2,n_3,S_4,S_5,j_3,T_2,T_3,T_4,T_5\}, \tag{A4}$$

which are compatible with K, T, J, and π. Even if in this work we use only two-body forces, this particular coupling scheme is very advantageous also when the three-nucleon interaction is included.

In terms of the states expressed in the jj-coupling scheme, the most generic NN potential matrix element is

$$V_{l\alpha,l'\alpha'}^{KLST,K'L'S'T',J\pi} = 15\sum_{\nu}\sum_{\nu'} B_{\alpha,\nu}^{KLSTJ\pi}\ B_{\alpha',\nu'}^{K'L'S'T'J\pi}\sum_{T_2^z} C_{T_3,T;T_3',T'}^{T_2,T_5;T_2^z}\ v_{l\nu_y,l'\nu_y'}^{K,K',j_1}(T_{2z})\delta_{\nu_x,\nu_x'}, \tag{A5}$$

where ν_x is defined as

$$\nu_x = \{j_1,n_4,\ell_4,j_2,j_{12},\ell_1,\ell_2,\ell_3,L_2,L_3,n_2,n_3,S_4,S_5,j_3,T_2,T_4,T_5\}, \tag{A6}$$

and

$$\nu_y = \{n_5,\ell_5,S_2\}. \tag{A7}$$

Note that $\nu \equiv \{\nu_x,\nu_y,T_3\}$. Moreover, we have defined the coefficients $C_{T_3,T;T_3',T'}^{T_2,T_5;T_{2z}}$, which come from the matrix elements of the isospin states, as

$$\begin{aligned}C_{T_3,T;T_3',T'}^{T_2,T_5;T_{2z}} = \sum_{T_{3z}T_{3z}'}&(T_3,T_{3z},T_5,T_z-T_{3z}|T,T_z)(T_3',T_{3z}',T_5,T_z-T_{3z}'|T,T_z)\\ &\times(T_2,T_{2z},T_5,T_{3z}-T_{2z}|T_3,T_{3z})(T_2,T_{2z},T_5,T_{3z}'-T_{2z}|T_3',T_{3z}'),\end{aligned} \tag{A8}$$

with $(\cdots|\cdots)$ the Clebsch-Gordan coefficients. The potential term $v_{l\nu_y,l'\nu_y'}^{K,K',j_1}(T_{2z})$ is the only part of Eq. (A5) which depends explicitly on the localityor nonlocality of the potential model. In the nonlocal case it is

$$\begin{aligned}v_{l\nu_y,l'\nu_y'}^{K,K',j_1}(T_{2z}) = \mathcal{N}_{n_5}^{\ell_5,\nu_5}\mathcal{N}_{n_5'}^{\ell_5',\nu_5'}\int_0^{\infty}d\rho_5\,\rho_5^{11}\int_0^{\infty}d\xi_5\,(\xi_5)^2\int_0^{\infty}d\xi_5'\,(\xi_5')^2 f_l(\rho)(\cos\varphi_5)^{\ell_5}(\sin\varphi_5)^{K_4}\\ \times P_{n_5}^{\nu_4,\ell_5+1/2}(\cos 2\varphi_5)v_{l_5S_2,l_5'S_2';j_1}^{T_{2z}}(\xi_5,\xi_5')\delta_{S_2,S_2'}f_{l'}(\rho')(\cos\varphi_5')^{\ell_5'}(\sin\varphi_5')^{K_4}P_{n_5'}^{\nu_4,\ell_5'+1/2}(\cos 2\varphi_5'),\end{aligned} \tag{A9}$$

where $\rho_5^2 = \xi_1^2+\xi_2^2+\xi_3^2+\xi_4^2$, $\rho^2 = \rho_5^2+\xi_5^2$, $(\rho')^2 = \rho_5^2+(\xi_5')^2$, $\cos\varphi_5 = \xi_5/\rho$, $\cos\varphi_5' = \xi_5'/\rho'$, and $v_{\ell S,\ell'S';j}^{T_{2z}}(\xi_5,\xi_5')$ is the nonlocal two nucleon potential acting between two-body states ${}^{2S+1}(\ell)_j$ and ${}^{2S'+1}(\ell')_j$ with isospin T_{2z}. The three dimensional integrals are then easily computed numerically with high accuracy with standard quadrature techniques. The local case can be easily derived by taking into account that

$$v_{l_5S_2,l_5'S_2';j_1}^{T_{2z}}(\xi_5,\xi_5') = \frac{\delta(\xi_5-\xi_5')}{\xi_5^2}v_{l_5S_2,l_5'S_2';j_1}^{T_{2z}}(\xi_5). \tag{A10}$$

The algorithm used to compute the NN potential matrix elements for the $A=6$ case is discussed in the next subsection.

2. Algorithmic implementation

Before starting to discuss the algorithm, let us give an idea of the dimension of the problem of computing the potential matrix elements in this formalism. We start from Eq. (A5). The number of operations needed to compute the potential matrix elements of Eq. (A5) for given sets $\gamma = \{K,L,S,T\}$ and $\gamma' = \{K',L',S',T'\}$ and fixed values of Laguerre indices l and l' would be in principle

$$N_{op}^{\gamma,\gamma'} \sim N_{\gamma}\times N_{\gamma'}\times N_{\nu}\times N_{\nu'}, \tag{A11}$$

where $N_{\gamma} \equiv M'_{KLSTJ\pi}$ is the total number of independent states as defined in Sec. II, and N_{ν} is the number of states entering the expansion given in Eq. (A2), which is of the order of $M_{KLSTJ\pi}$. For example, if we consider $\gamma = \gamma' = \{12,2,1,0\}$ which is one of the worst cases, we have $N_{\gamma} = N_{\gamma'} \approx 10^3$ and $N_{\nu} = N_{\nu'} \approx 2.3\times 10^6$ then $N_{op}^{\gamma,\gamma'} \approx 5\times 10^{18}$. Let us suppose we are in an ideal case in which the time required for any of this operation is the typical clock time of a computer, 10^{-9} s, and that we are able to use in parallel 10^3 nodes. The total time required for doing all these operations is

$$T_{op}^{\gamma,\gamma'} \approx 58 \text{ days}, \tag{A12}$$

which is a time too long for any practical purpose, especially if we need to repeat these operations for all the possible combinations of states γ, γ', of Laguerre polynomials l, l' and all the potential models we want to study. For this reason we introduce the coefficients D, as follows.

As it can be seen from Eq. (A9), the potential integrals $v^{K,K',j_1}_{l\nu_y,l'\nu'_y}(T_{2z})$ depend only on the index of the Laguerre polynomials and the quantum numbers T_{2z}, K, K', j_1, ν_y, and ν'_y, where we remember that $\nu_y = \{n_5, \ell_5, S_2\}$. Therefore, Eq. (A5) can be rewritten in a more convenient form as

$$V^{\gamma,\gamma';J\pi}_{l\alpha,l'\alpha'} = 15 \sum_{\nu_y,\nu'_y} \sum_{T_3,T'_3} D^{\gamma,\gamma';J\pi}_{\alpha,\nu_y T_3;\alpha',\nu'_y T'_3} \times \sum_{T_{2z}} C^{T_2,T_5;T_{2z}}_{T_3,T;T'_3,T'} v^{K,K',j_1}_{l\nu_y,l'\nu'_y}(T_{2z}), \tag{A13}$$

where we denote $D^{\gamma,\gamma';J\pi}_{\alpha,\nu_y T_3;\alpha',\nu'_y T'_3}$ the D coefficient, and its expression can be easily derived comparing Eq. (A5) with Eq. (A13). Above, α (α') defined in Eq. (14), corresponds to one of the N_γ ($N_{\gamma'}$) independent states. Explicitly the D coefficients are given by

$$D^{\gamma,\gamma',J\pi}_{\alpha,\nu_y T_3;\alpha',\nu'_y T'_3} = \sum_{\nu_x\nu'_x} B^{\gamma J\pi}_{\alpha,\nu_y T_3 \nu_x} B^{\gamma' J\pi}_{\alpha',\nu'_y T'_3 \nu'_x} \delta_{\nu_x\nu'_x}, \tag{A14}$$

where ν_x are given in Eq. (A6). In this way the only parts which depend on the nuclear interaction in Eq. (A13) are the potential integrals $v^{K,K'}_{l\nu_y,l'\nu'_y}(T_{2z})$, while the coefficients defined in Eq. (A14) do not. Therefore, we can compute and store the D coefficients only once for all.

This can be further simplified since for all the possible states α and α' with fixed γ and γ', the states ν and ν' giving a nonvanishing contribution are always the same. In other words, the determination of the pair of states ν, ν' that fulfill the condition $\delta_{\nu_x\nu'_x}$, which in general requires $N_\nu \times N_{\nu'}$ operations, can be performed only once for all the combinations α, α' and requires a typical time of 10–20 minutes for $10 \leqslant K, K' \leqslant 14$ using a single node with 48 CPUs working in parallel. The number of operations which remain to be done in Eq. (A14) is then equal to the number of states ν_x (N_{ν_x}). Therefore, $N^{\gamma,\gamma'}_{op}$ reduces to

$$N^{\gamma,\gamma'}_{op} \sim N_\gamma \times N_{\gamma'} \times N_V \times N_{\nu_x}, \tag{A15}$$

where N_V is the number of combinations ν_y, ν'_y permitted by the potential, which is typically <200. The $N^{\gamma,\gamma'}_{op}$ in this case is then orders of magnitude smaller than the value given in Eq. (A11). In a realistic situation, the typical time required for the computation of Eq. (A14), namely to perform the $N_V \times N_{\nu_x}$ operations, is $T_D \approx 0.1$ s. Therefore, for $\gamma = \gamma' = \{12, 2, 1, 0\}$,

$$T^{\gamma,\gamma'}_{op} \sim N_\gamma \times N_{\gamma'} \times T_D \approx 1 \text{ day}, \tag{A16}$$

using a computer with 48 CPUs on a single node.

In Fig. 7 we report the total time needed to compute the D coefficients when $L = L' = 0$, $S = S' = 1$ and $T = T' = 0$ up to given $K = K' = K_{\max}$, namely

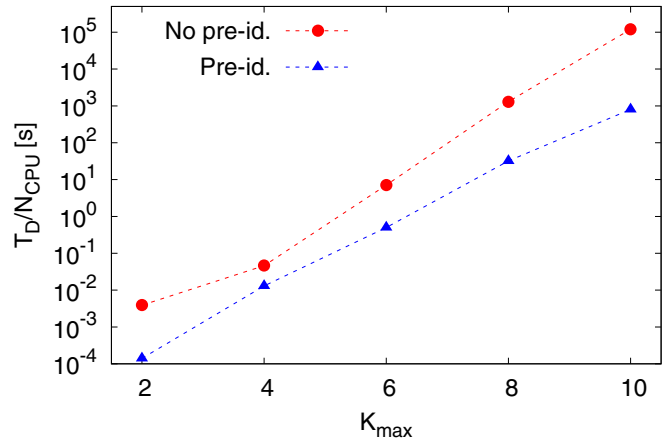

FIG. 7. Total time needed to compute the D coefficients [Eq. (A17)] as function of $K = K' = K_{\max}$ divided by N_{CPU}, the number of CPUs used in the computation. These calculations are performed for fixed values of the other quantum numbers, in particular $L = L' = 0$, $S = S' = 1$, and $T = T' = 0$. The red dots are the time spent without pre-identification, while the blue triangles are the time spent with pre-identification. The dashed lines are added to guide the eyes. The calculations were performed on a single node with 48 Intel Xenon 8160 CPUs at 2.10 GHz (i.e., $N_{CPU} = 48$).

$$T_D = \sum_{K=2}^{K_{\max}} \sum_{K'=2}^{K_{\max}} T^{K010,K'010}_{op}, \tag{A17}$$

divided by the number of CPUs (N_{CPU}) used in the computation. In particular, the blue triangles give T_D by using first the pre-identification of the pair of states ν, ν' to fulfill the δ_{ν_x,ν'_x} condition as discussed before, while the red dots correspond to the time spent without pre-identification. As is clear from the figure, the computational time increases exponentially by increasing the values of $K_{\max}$, since it is proportional to the number of independent states, which grows exponentially as well. However, by using the pre-identification, not only is T_D well reduced, but also as function of $K_{\max}$ it has a minor slope compared to the case without pre-identification. The exponential growth limits the maximum value of $K_{\max}$ we can use at present. However, we expect to have a great improvement by using a larger number of CPUs distributing the calculation on several nodes.

Regarding the storage, the total memory required for fixed γ and γ' is given by the number of D coefficients for each α, α' combination, namely

$$M_{\gamma,\gamma'}[\text{GB}] \sim 3 \times \frac{8 \times N_\gamma \times N_{\gamma'} \times N_V}{1024^3}, \tag{A18}$$

where the factor 3 is an empirical factor, which takes care of the additional information needed in the files to save the coefficients D. For example, when $\gamma = \gamma' = \{12, 2, 1, 0\}$, the size of the file is only 2.2 GB. The total memory we used to store all the D coefficients used for computing the ^{6}Li ground state in this work is ≈100 GB.

Once the D coefficients are computed, the time required for the calculation of all the potential matrix elements is

of the order of a couple of hours. Indeed we need only to compute the sum over the combinations ν_y, ν'_y allowed by the potential (N_V), which are very few for all the possible γ, γ' and l, l'. This process can be even accelerated by computing and storing the matrix elements of Eq. (A9) before combining them with the D coefficients.

Typically, in the *ab initio* methods, the potential matrix elements are computed and stored for each potential model. By using our approach, we are able to save only the D coefficients by eliminating the dependence on the potential models.

APPENDIX B: HH EXPANSION OF THE SOURCE TERM

In this Appendix we present the explicit derivation of the source term as given in Eq. (62).

As discussed in the text, in order to simplify the calculation we expand the cluster part of Eq. (62) in terms of the HH functions [see Eq. (63)]. Before doing that, we need to eliminate the δ function in Eq. (62) by expanding $g_L(r)$ in terms of the Laguerre polynomials, i.e.,

$$g_L(r) = \sum_{n=0}^{N_{\max}} C_n^L \overline{f}_n(r), \tag{B1}$$

where

$$\overline{f}_n(r) = \gamma_a^{\frac{3}{2}} \sqrt{\frac{n!}{(n+2)!}} L_n^{(2)}(\gamma_a r) e^{-\frac{\gamma_a r}{2}}. \tag{B2}$$

The parameter γ_a is chosen to optimize the expansion. Then, the coefficients C_n^L are given by

$$C_n^L = \int dr\, r^2 g_L(r) \overline{f}_n(r), \tag{B3}$$

and, substituting Eq. (62) in Eq. (B3), we obtain

$$\begin{aligned} C_n^L = \sqrt{15}\left(\frac{\sqrt{6}}{4}\right)^{\frac{3}{2}} \int \prod_{i=1,5} d\boldsymbol{\xi}_{iB}\, \Psi_{^6\mathrm{Li}}(\boldsymbol{\xi}_{1B}, \ldots, \boldsymbol{\xi}_{5B})^\dagger \\ \times \left(\sum_{i\in\alpha}\sum_{j\in d} V_{ij} - \frac{2e^2}{r}\right) \big[(\Psi_\alpha(\boldsymbol{\xi}_{3B}, \boldsymbol{\xi}_{4B}, \boldsymbol{\xi}_{5B}) \\ \times \Psi_d(\boldsymbol{\xi}_{1B}))_1 Y_L(\hat{r})\big]_1 \overline{f}_n(r)\Big|_{\boldsymbol{r}=\sqrt{\frac{3}{8}}\boldsymbol{\xi}_{2B}}. \end{aligned} \tag{B4}$$

If now we define the 4+2 cluster wave function as

$$\Psi_{L,n} = [(\Psi_\alpha(\boldsymbol{\xi}_{3B}, \boldsymbol{\xi}_{4B}, \boldsymbol{\xi}_{5B}) \times \Psi_d(\boldsymbol{\xi}_{2B}))_1 Y_L(\hat{r})]_1 \overline{f}_n(r). \tag{B5}$$

it is possible to expand it in terms of the six-body HH states, namely

$$\Psi_{L,n} = \sum_{\overline{l}=0}^{\overline{l}_{\max}} \sum_{\overline{K}=0}^{\overline{K}_{\max}} \sum_{\overline{L}\overline{S}\overline{T},\overline{\alpha}} c_{\overline{l},\overline{\alpha}}^{\overline{K}\overline{L}\overline{S}\overline{T}}(L,n) \sum_{p_\alpha=1}^{12} \Phi_{\overline{l},\overline{\alpha}}^{\overline{K}\overline{L}\overline{S}\overline{T}}(p_\alpha), \tag{B6}$$

where we have defined

$$\Phi_{\overline{l},\overline{\alpha}}^{\overline{K}\overline{L}\overline{S}\overline{T}}(p) = f_{\overline{l}}(\rho) \Phi_{\overline{\alpha}}^{\overline{K}\overline{L}\overline{S}\overline{T}}(i,j,k,l,m,n), \tag{B7}$$

with $\Phi_{\overline{\alpha}}^{\overline{K}\overline{L}\overline{S}\overline{T}}$ the HH functions of Eq. (13) expressed in terms of the set "B" of Jacobi coordinates, and $f_{\overline{l}}(\rho)$ the hyperradial function of Eq. (25). Note that with p_α we indicate the even permutation of (i,j,k,l) of the six particles $(i,j,k,l,5,6)$ which coincide with the 12 permutations of the four particles inside the α particle. In Eq. (B6) the coefficients $c_{\overline{l},\overline{\alpha}}^{\overline{K}\overline{L}\overline{S}\overline{T}}(L,n)$ are obtained from

$$c_{\overline{l},\overline{\alpha}}^{\overline{K}\overline{L}\overline{S}\overline{T}}(L,n) = \left\langle \Phi_{\overline{l},\overline{\alpha}}^{\overline{K}\overline{L}\overline{S}\overline{T}}(p=1) \middle| \Psi_{L,n}(p=1) \right\rangle_{\Omega_B,\rho}, \tag{B8}$$

where with $\langle\rangle_{\Omega_B,\rho}$ we indicate the integration over all the internal variables and the spin-isospin traces. These coefficients are exactly the $c_{[\overline{K}],\overline{l}}$ coefficients defined in Eq. (63). We want to underline that the calculation of these coefficients is very easy since it involves only the reference permutation ($p=1$). The equivalence in Eq. (B6) holds exactly only when $\overline{K}_{\max} \to \infty$ and $\overline{l}_{\max} \to \infty$. Obviously this is not the case, but we can check the quality of our expansion by looking to the convergence of the observables when we increase $\overline{K}_{\max}$ and $\overline{l}_{\max}$. By replacing Eq. (B6) in Eq. (B4) the calculation of the source term reduces to computing a series of matrix elements of the potential between HH states, that can be easily done by following the procedure of Appendix A.

For the calculation of the source term we use $N_{\max} = 20$ for the expansion with the Laguerre polynomials of the source term [Eq. (B1)] and $\overline{l}_{\max} = 40$ for the hyperradial part of the cluster function [Eq. (B6)]. Both these values permit reaching full convergence in the respective expansions. The study of the convergence as function of $\overline{K}$ is discussed in the main text.

[1] J. Carlson, S. Gandolfi, F. Pederiva, S. C. Pieper, R. Schiavilla, K. E. Schmidt, and R. B. Wiringa, Rev. Mod. Phys. **87**, 1067 (2015).

[2] M. Piarulli, A. Baroni, L. Girlanda, A. Kievsky, A. Lovato, E. Lusk, L. E. Marcucci, S. C. Pieper, R. Schiavilla, M. Viviani, and R. B. Wiringa, Phys. Rev. Lett. **120**, 052503 (2018).

[3] S. K. Bogner, R. J. Furnstahl, and R. J. Perry, Phys. Rev. C **75**, 061001(R) (2007).

[4] E. D. Jurgenson, P. Navrátil, and R. J. Furnstahl, Phys. Rev. Lett. **103**, 082501 (2009).

[5] B. R. Barrett, P. Navrátil, and J. P. Vary, Prog. Part. Nucl. Phys. **69**, 131 (2013).

[6] N. Barnea, W. Leidemann, and G. Orlandini, Phys. Rev. C **61**, 054001 (2000).

[7] N. Barnea, W. Leidemann, and G. Orlandini, Phys. Rev. C **81**, 064001 (2010).

[8] S. Vaintraub, N. Barnea, and D. Gazit, Phys. Rev. C **79**, 065501 (2009).

[9] M. Gattobigio, A. Kievsky, and M. Viviani, Phys. Rev. C **83**, 024001 (2011).

[10] A. Shirokov, J. Vary, A. Mazur, and T. Weber, Phys. Lett. B **644**, 33 (2007).

[11] A. Volkov, Nucl. Phys. **74**, 33 (1965).

[12] K. Varga and Y. Suzuki, Phys. Rev. C **52**, 2885 (1995).

[13] J. Lazauskas and R. Carbonell, Few-Body Syst. **60**, 62 (2019).
[14] R. Lazauskas and J. Carbonell, Front. Phys. **7**, 251 (2020).
[15] A. Kievsky, S. Rosati, M. Viviani, L. Marcucci, and L. Girlanda, J. Phys. G: Nucl. Part. Phys. **35**, 063101 (2008).
[16] L. E. Marcucci, J. Dohet-Eraly, L. Girlanda, A. Gnech, A. Kievsky, and M. Viviani, Front. Phys. **8**, 69 (2020).
[17] V. Efros, Sov. J. Nucl. Phys. **15**, 128 (1972).
[18] V. Efros, Sov. J. Nucl. Phys. **27**, 448 (1979).
[19] V. Demin, Sov. J. Nucl. Phys. **26**, 379 (1977).
[20] M. F. de la Ripelle, Ann. Phys. (NY) **147**, 281 (1983).
[21] M. Viviani, A. Kievsky, and S. Rosati, Phys. Rev. C **71**, 024006 (2005).
[22] M. Viviani, Few-Body Syst. **25**, 177 (1998).
[23] J. Dohet-Eraly and M. Viviani, Comp. Phys. Commun. **253**, 107183 (2020).
[24] F. Zernike and H. Brinkman, Proc. Kon. Ned. Acad. Wensch. **33**, 3 (1935).
[25] M. Abramowitz and I. Stegun, *Handbook of Mathematical Functions* (Dover, New York, 1970).
[26] J. Cullum and R. Willoughby, J. Comput. Phys. **44**, 329 (1981).
[27] D. R. Entem and R. Machleidt, Phys. Rev. C **68**, 041001(R) (2003).
[28] V. Zakharyev, B. N. Pustovalov and E. Efros, Sov. J. Nucl. Phys. **8**, 234 (1969).
[29] T. Schneider, Phys. Lett. B **40**, 439 (1972).
[30] E. D. Jurgenson, P. Navrátil, and R. J. Furnstahl, Phys. Rev. C **83**, 034301 (2011).
[31] I. Stetcu, B. R. Barrett, P. Navrátil, and J. P. Vary, Phys. Rev. C **71**, 044325 (2005).
[32] J. L. Friar, J. Martorell, and D. W. L. Sprung, Phys. Rev. A **56**, 4579 (1997).
[33] L. Foldy and S. Wouthuysen, Phys. Rev. **78**, 29 (1950).
[34] M. Tanabashi and *et al.* (Particle Data Group), Phys. Rev. D **98**, 030001 (2018).
[35] M. Puchalski and K. Pachucki, Phys. Rev. Lett. **111**, 243001 (2013).
[36] N. Stone, *Table of Nuclear Magnetic Dipole and Electric Quadrupole Moments* (IAEA, Vienna, 2014) and references therein.
[37] J. Carlson and R. Schiavilla, Rev. Mod. Phys. **70**, 743 (1998).
[38] R. Schiavilla, A. Baroni, S. Pastore, M. Piarulli, L. Girlanda, A. Kievsky, A. Lovato, L. E. Marcucci, S. C. Pieper, M. Viviani, and R. B. Wiringa, Phys. Rev. C **99**, 034005 (2019).
[39] J. L. Forest, V. R. Pandharipande, S. C. Pieper, R. B. Wiringa, R. Schiavilla, and A. Arriaga, Phys. Rev. C **54**, 646 (1996).
[40] K. M. Nollett, R. B. Wiringa, and R. Schiavilla, Phys. Rev. C **63**, 024003 (2001).
[41] P. Navrátil, Phys. Rev. C **70**, 054324 (2004).
[42] P. Navrátil and S. Quaglioni, Phys. Rev. C **83**, 044609 (2011).
[43] G. Hupin (private communication).
[44] G. Hupin, S. Quaglioni, and P. Navrátil, Phys. Rev. Lett. **114**, 212502 (2015).
[45] E. A. George and L. D. Knutson, Phys. Rev. C **59**, 598 (1999).
[46] R. G. H. Robertson, P. Dyer, R. A. Warner, R. C. Melin, T. J. Bowles, A. B. McDonald, G. C. Ball, W. G. Davies, and E. D. Earle, Phys. Rev. Lett. **47**, 1867 (1981).
[47] R. Machleidt, Phys. Rev. C **63**, 024001 (2001).
[48] N. Timofeyuk, Nucl. Phys. A **632**, 19 (1998).
[49] R. B. Wiringa, V. G. J. Stoks, and R. Schiavilla, Phys. Rev. C **51**, 38 (1995).
[50] B. S. Pudliner, V. R. Pandharipande, J. Carlson, S. C. Pieper, and R. B. Wiringa, Phys. Rev. C **56**, 1720 (1997).
[51] A. H. Abdelhameed, G. Angloher, P. Bauer, A. Bento, E. Bertoldo, C. Bucci, L. Canonica, A. D'Addabbo, X. Defay *et al.*, Eur. Phys. J. C **79**, 630 (2019).
[52] J. Lewin and P. Smith, Astropart. Phys. **6**, 87 (1996).
[53] C. Körber, A. Nogga, and J. de Vries, Phys. Rev. C **96**, 035805 (2017).